The Role of Elevated Terrain and the Gulf of Mexico in the Production of Severe Local Storm Environments over North America

FUNING LI,[a] DANIEL R. CHAVAS,[a] KEVIN A. REED,[b] NAN ROSENBLOOM,[c] AND DANIEL T. DAWSON II[a]

[a] *Purdue University, Department of Earth, Atmospheric, and Planetary Sciences, West Lafayette, Indiana*
[b] *School of Marine and Atmospheric Sciences, Stony Brook University, Stony Brook, New York*
[c] *National Center for Atmospheric Research, Boulder, Colorado*

(Manuscript received 31 July 2020, in final form 12 May 2021)

ABSTRACT: The prevailing conceptual model for the production of severe local storm (SLS) environments over North America asserts that upstream elevated terrain and the Gulf of Mexico are both essential to their formation. This work tests this hypothesis using two prescribed-ocean climate model experiments with North American topography removed or the Gulf of Mexico converted to land and analyzes how SLS environments and associated synoptic-scale drivers (southerly Great Plains low-level jets, drylines, elevated mixed layers, and extratropical cyclones) change relative to a control historical run. Overall, SLS environments depend strongly on upstream elevated terrain but more weakly on the Gulf of Mexico. Removing elevated terrain substantially reduces SLS environments especially over the continental interior due to broad reductions in both thermodynamic instability and vertical wind shear, leaving a more zonally uniform residual distribution that is maximized near the Gulf coast and decays toward the continental interior. This response is associated with a strong reduction in synoptic-scale drivers and a cooler and drier mean-state atmosphere. Replacing the Gulf of Mexico with land modestly reduces SLS environments over the Great Plains (driven primarily thermodynamically) and increases them over the eastern United States (driven primarily kinematically), shifting the primary local maximum eastward into Illinois; it also eliminates the secondary, smaller local maximum over southern Texas. This response is associated with modest changes in synoptic-scale drivers and a warmer and drier lower troposphere. These experiments provide insight into the role of elevated terrain and the Gulf of Mexico in modifying the spatial distribution and seasonality of SLS environments.

KEYWORDS: Wind shear; Convective storms; Storm environments; Thermodynamics; General circulation models

1. Introduction

Eastern North America is one of the most prominent hotspots globally for severe local storm (SLS) events, including those that produce damaging winds, large hailstones, and/or tornadoes (Ludlam 1963; Johns and Doswell 1992; Brooks et al. 2003). Although SLS events are small scale, they develop principally within favorable larger-scale environments (Brooks et al. 2003). These environments are commonly defined using proxies that combine key thermodynamic and kinematic ingredients, particularly: 1) the product of convective available potential energy (CAPE) and 0–6-km bulk vertical wind shear (S06), and 2) the 0–3-km energy helicity index (EHI03) that is proportional to the product of CAPE and 0–3-km storm relative helicity (SRH03) (Rasmussen and Blanchard 1998; Rasmussen 2003; Brooks et al. 2003; Doswell and Schultz 2006; Grams et al. 2012). Deep convection may be initiated when air parcels reach their level of free convection; if convective inhibition (CIN) exists this process may be delayed owing to the suppression of upward motion by the associated stable layer, allowing CAPE to build up prior to initiation (Colby 1984; Williams and Renno 1993; Agard and Emanuel 2017; Chen et al. 2020). Large-scale ascent and synoptic-scale dynamics such as convergence along air mass boundaries (e.g., synoptic fronts and drylines) and orographic lifting are all efficient ways to initiate convective storms (Markowski and Richardson 2011). SLS environments over North America are generally confined to the eastern half of the United States, especially the Great Plains (Brooks et al. 2003; Gensini and Ashley 2011; Li et al. 2020), although recent studies have indicated changes in their spatial distribution in past decades (Gensini and Brooks 2018; Tang et al. 2019; Taszarek et al. 2021a).

The climatology of SLS environments generally aligns well with that of observed SLS activity in the United States, including their broadly consistent annual spatial patterns and strong seasonal and diurnal cycles (Gensini and Ashley 2011; Agee et al. 2016; Gensini and Brooks 2018; Tang et al. 2019; Taszarek et al. 2020, 2021a,b). Thus, improving our understanding of what factors generate SLS environments in the first place can help us better understand SLS activity on climate time scales. Moreover, the larger-scale nature of these environments allows for the use of reanalysis data (Brooks et al. 2003; Gensini and Ashley 2011; Allen and Karoly 2014; Gensini et al. 2014; Tippett et al. 2016; Gensini and Brooks 2018; Taszarek et al. 2018; Tang et al. 2019; Taszarek et al. 2020, 2021a,b) and global climate models (Diffenbaugh et al. 2013; Tippett et al. 2015; Seeley and Romps 2015; Hoogewind et al. 2017; Chen et al. 2020; Li et al. 2020), which can resolve SLS environments though not actual SLS events. To date, though, global climate model experiments have yet to be applied to test how SLS environments are generated over North

Supplemental information related to this paper is available at the Journals Online website: https://doi.org/10.1175/JCLI-D-20-0607.s1.

Corresponding author: Funing Li, li3226@purdue.edu

DOI: 10.1175/JCLI-D-20-0607.1

America in the present climate state in the first place, which limits our ability to predict how SLS activity may change due to climate change.

The prevailing conceptual model for the generation of SLS environments over the eastern United States was proposed by Carlson et al. (1983) (Fig. 1). This model identifies elevated terrain to the west and the Gulf of Mexico to the south as the key geographic features essential to producing these environments. First, the Gulf of Mexico provides a source of warm and moist low-level air. Second, surface heating of the Colorado and Mexican plateaus upstream generates well-mixed (dry adiabatic) layers aloft characterized by steep lapse rates. SLS environments then arise downstream of the elevated terrain due to the superposition of these two layers. In reality, this superposition is typically mediated by synoptic-scale features including southerly Great Plains low-level jets (GPLLJs), drylines, elevated mixed layers (EMLs), and extratropical cyclones. Specifically, southerly GPLLJs enhance the inland transport of warm and moist low-level air from the Gulf of Mexico, especially during the nighttime in spring and summer (Bonner 1968; Helfand and Schubert 1995; Whiteman et al. 1997; Higgins et al. 1997; Weaver and Nigam 2008; Weaver et al. 2012). Meanwhile, the westerly jet stream advects well-mixed air overlying the elevated terrain downstream. This process creates meridionally oriented drylines over the Great Plains when the descending dry air encounters the moist near-surface air from the Gulf of Mexico (Fujita 1958; Schaefer 1974; Ziegler and Hane 1993; Hoch and Markowski 2005). Farther east, this process also produces an EML over the moist low-level air that commonly forms strong capping inversions and creates CIN that inhibits convective initiation for boundary layer parcels (Carlson et al. 1983; Lanicci and Warner 1991a; Banacos and Ekster 2010). This can allow for a strong buildup of CAPE during the daytime heating (Carlson et al. 1983; Farrell and Carlson 1989; Lanicci and Warner 1991b,c; Cordeira et al. 2017; Ribeiro and Bosart 2018). Moreover, the above model implicitly assumes differential advection of two layers and thus is associated with vertical wind shear. These CAPE- and shear-producing processes are often strongly amplified locally in the presence of a surface extratropical cyclone (Doswell and Bosart 2001; Hamill et al. 2005; Tochimoto and Niino 2015), whose formation is favored downstream of the Rocky Mountains (Held et al. 2002; Brayshaw et al. 2009). In combination, the result is the production of SLS environments characterized by high values of CAPE and shear.

Previous studies partially tested this conceptual model using limited-area numerical model experiments but focused principally on the role of elevated terrain (Benjamin and Carlson 1986; Benjamin 1986; Arritt et al. 1992; Rasmussen and Houze 2016). Benjamin and Carlson (1986) tested the key role of elevated terrain for two historical SLS outbreaks over the Great Plains in a regional mesoscale modeling framework. Benjamin (1986) and Arritt et al. (1992) further examined effects of elevated terrain on the production of strong capping inversions downstream based on two-dimensional idealized experiments. Rasmussen and Houze (2016) found a strong orographic control on convective initiation downstream of the Andes over South America via high-resolution simulations of a convective

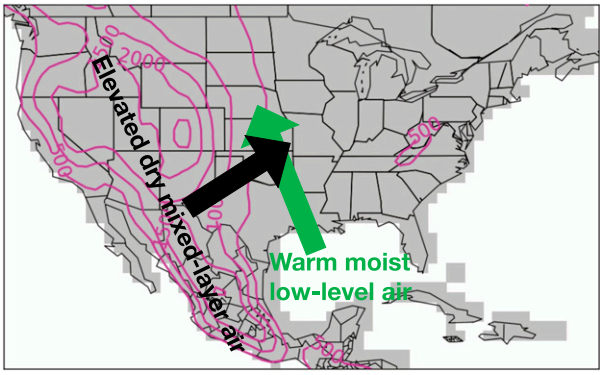

FIG. 1. Schematic diagram of the conceptual model by Carlson et al. (1983) representing conditions favorable for the formation of severe local storm environments over the central United States. Contour lines indicate elevation (m).

system from the Weather Research and Forecasting Model, and indicated a conceptual model for the production of SLS environments in subtropical South America that is similar to the U.S. Great Plains. Additionally, various numerical model experiments with terrain modifications have shown substantial impacts of orography on larger-scale atmospheric flows including GPLLJs (Pan et al. 2004; Ting and Wang 2006) and stationary waves or storm tracks (Broccoli and Manabe 1992; Held et al. 2002; Inatsu et al. 2002; Brayshaw et al. 2009; Chang 2009; Wilson et al. 2009; Sandu et al. 2019; Lutsko et al. 2019). However, this conceptual model, including both upstream elevated terrain and the Gulf of Mexico, has yet to be tested using global climate model experiments.

Thus, this work aims to explicitly test the conceptual model of Carlson et al. (1983) using a global climate model [the Community Atmosphere Model version 6 (CAM6)] by addressing the following questions:

1) How important are western North American elevated terrain and the Gulf of Mexico for producing SLS environments? Do they affect the seasonality of these environments?
2) How are these responses of SLS environments associated with responses of SLS-relevant synoptic-scale features in each experiment?
3) How are these responses of SLS environments and SLS-relevant synoptic-scale features associated with changes in the mean state and characteristic synoptic flow patterns in each experiment?

To answer these questions, we perform numerical experiments using CAM6, in which we flatten topography over North America or convert the Gulf of Mexico to land, respectively. This work serves as a direct assessment of the geographic controls of SLS environments to help better understand the formation of these environments within Earth's climate system. These experiments are compared against a control historical simulation presented in Li et al. (2020, hereafter L20). L20 found that CAM6 can broadly reproduce the climatology of SLS environments and associated synoptic-scale features

over North America, as compared to the ERA5 reanalysis dataset. L20 also noted a few key biases in CAM6, including a high bias in CAPE over the eastern third of the United States associated with the systematic warm and moist biases that are known to persist across many regional and global climate models (Klein et al. 2006; Cheruy et al. 2014; Mueller and Seneviratne 2014; Seeley and Romps 2015; Lin et al. 2017; Qian et al. 2020).

Section 2 describes our experimental design and analysis methodology. Section 3 analyzes the responses of SLS environments, the associated synoptic-scale features, and the synoptic flow patterns to removing elevated terrain. Section 4 analyzes these responses to filling the Gulf of Mexico. Finally, section 5 summarizes key conclusions and discusses avenues for future work.

2. Methodology

a. Experimental design

We use CAM6 as our experimental laboratory for this study. CAM6 is the atmospheric component of the Community Earth System Model version 2.1 (available at http://www.cesm.ucar.edu/models/cesm2/) developed in part for participation in phase 6 of the Coupled Model Intercomparison Project (CMIP6; Eyring et al. 2016). Compared with its predecessor CAM5 (Neale et al. 2012), CAM6 contains substantial improvements to the physical parameterization suite: schemes for boundary layer turbulence, shallow convection, and cloud macrophysics in CAM5 are replaced by the Cloud Layers Unified by Binormals (CLUBB; Golaz et al. 2002; Bogenschutz et al. 2013) scheme; the improved two-moment prognostic cloud microphysics from Gettelman and Morrison (2015), which carries prognostic precipitation species (rain and snow) in addition to cloud condensates, is included; and the orographic drag parameterizations are also updated. CAM6 uses the Zhang and McFarlane (1995) scheme for deep convection parameterization, in which a measure of entraining CAPE serves as both trigger and mass flux closure for deep convection. The convective scheme is triggered when this entraining CAPE exceeds $70\,\mathrm{J\,kg^{-1}}$ and the CAPE-based closure assumes that convection consumes CAPE with characteristic time scale $\tau = 1$ h. The entraining CAPE used in the Zhang and McFarlane (1995) scheme includes the effect of lateral entrainment dilution (Neale et al. 2008), which allows for mixing of the rising plume with surrounding environmental air. It is also defined as the integrated buoyancy starting from the parcel level, rather than its level of free convection, for a parcel at the level of maximum moist static energy within planetary boundary layer; hence, CIN is included in the buoyancy integral. Because of these differences, the entraining CAPE in the convective scheme can be much smaller than the traditional definition of CAPE used in this work [defined below in Eq. (3)], which can allow for large values of CAPE to exist without triggering the convection scheme. In addition, the standard Zhang and McFarlane (1995) scheme in CAM6 is modified by the addition of convective momentum transport (Richter and Rasch 2008), and has been retuned compared to earlier versions in CAM predecessors to increase the sensitivity to convective initiation.

We define as our control simulation (CTRL) an Earth-like climate state over the period 1979–2014, following the Atmospheric Model Intercomparison Project (AMIP) protocols (Gates et al. 1999). This CTRL run is exactly the same simulation we performed and evaluated in L20 and was found capable of reproducing the climatology of SLS environments and the associated synoptic-scale features over North America. A similar setup was also examined in previous work with CAM5 (Wehner et al. 2014; Varuolo-Clarke et al. 2019). CAM6 is configured with the default finite-volume dynamical core on a $0.9° \times 1.25°$ latitude–longitude grid mesh. The simulation reaches its equilibrium state quickly in terms of the steady temporal evolution of surface heat fluxes over the eastern United States, western United States, and the Gulf of Mexico, respectively (see Figs. S1a,b in the online supplemental material). Thus, we only discard the first year for spinup and analyze the 3-hourly output from 1980 to 2014.

In addition to CTRL, we perform two experiments to investigate the role of elevated terrain and the Gulf of Mexico in producing SLS environments over North America. In the first experiment, we set North American topography to zero (i.e., elevation = 0 m; Fig. 2b) without changing land cover type (the "noTOPO" experiment). In the second experiment, we fill in the Gulf of Mexico by replacing ocean cells in the Gulf of Mexico with land (Fig. 2c; denoted as the "noGOM" experiment). In addition to the modified land mask, we set the plant functional type (PFT) to C4 grass in the Community Land Model version 5 (CLM5; Lawrence et al. 2018) over this "new land" for simplicity, and hence may be considered as a low-lying plain covered by grass. This added grassland strongly increases surface sensible heat flux (from ~10 $\mathrm{W\,m^{-2}}$ in CTRL to up to 100 $\mathrm{W\,m^{-2}}$ in noGOM) and decreases surface latent heat flux (from ~200 $\mathrm{W\,m^{-2}}$ in CTRL to less than 100 $\mathrm{W\,m^{-2}}$ in noGOM) over the Gulf of Mexico during warm seasons (Figs. S1a,b vs Figs. S1e,f), consistent with differences in the surface energy budget over land and ocean. Ultimately we do not know what the true land type would be if the Gulf of Mexico were land, and existing research suggests significant intrinsic uncertainty given that subtropical land surfaces can have multiple stable states (Rietkerk et al. 2011; Staver et al. 2011). Future work could test the effects of filling the Gulf of Mexico with different, or a combination of, land types. Similar to CTRL, we perform both noTOPO and noGOM experiments over the period 1979–2014 and analyze the 3-hourly output from 1980 to 2014 when the model is in steady state (Figs. S1c–f).

b. Analysis

1) SLS environments

Our analyses focus on responses of the climatology of SLS environments in noTOPO and noGOM each as compared to CTRL. For the purposes of this study, we define SLS environments as the 99th percentile of two combined proxies, CAPES06 (Brooks et al. 2003) and EHI03 (Hart and Korotky 1991; Davies-Jones 1993), as well as their constituent parameters. Specifically,

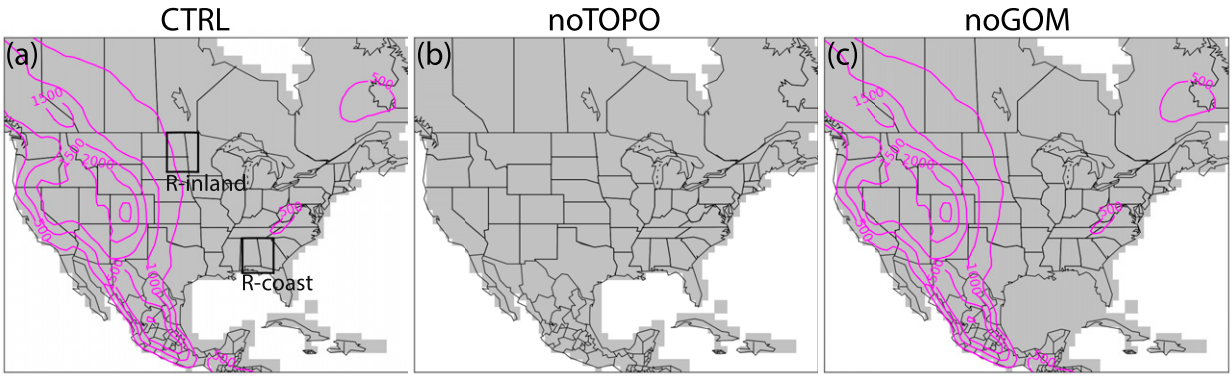

FIG. 2. Elevation (m; contour lines) and land mask (filled gray) for (a) CTRL, (b) noTOPO, and (c) noGOM. R-inland and R-coast in (a) denote the two 5° × 5° subregion boxes selected for regional analysis.

CAPES06 is the product of surface-based CAPE (Doswell and Rasmussen 1994) and S06 (Rasmussen and Blanchard 1998; Weisman and Rotunno 2000); EHI03 is a dimensionless quantity proportional to the product of surface-based CAPE and SRH03 and is a proxy for the potential for updraft rotation (Davies-Jones et al. 1990). We also analyze surface-based CIN (Colby 1984; Williams and Renno 1993; Riemann-Campe et al. 2009), which permits the buildup of CAPE. Calculations of these proxies and parameters use the following equations:

$$\mathrm{CAPES06} = \mathrm{CAPE} \times \mathrm{S06}, \tag{1}$$

$$\mathrm{EHI03} = \frac{\mathrm{CAPE} \times \mathrm{SRH03}}{160\,000\ \mathrm{m^4\ s^{-4}}}, \tag{2}$$

$$\mathrm{CAPE} = \int_{z_{\mathrm{LFC}}}^{z_{\mathrm{EL}}} g \frac{T_{vp} - T_{ve}}{T_{ve}} dz, \tag{3}$$

$$\mathrm{S06} = |\mathbf{V}_{6\mathrm{km}} - \mathbf{V}_{10\mathrm{m}}|, \tag{4}$$

$$\mathrm{SRH03} = -\int_{z_b}^{z_t} \hat{\mathbf{k}} \cdot (\mathbf{V} - \mathbf{C}) \times \frac{\partial \mathbf{V}}{\partial z} dz, \tag{5}$$

$$\mathrm{CIN} = -\int_{z_p}^{z_{\mathrm{LFC}}} g \frac{T_{vp} - T_{ve}}{T_{ve}} dz, \tag{6}$$

where $g = 9.81\ \mathrm{m\ s^{-2}}$ is the acceleration due to gravity, z_{LFC} and z_{EL} denote the level of free convection and the equilibrium level, $z_p = 2$ m defines the height of the near-surface parcel, T_{vp} and T_{ve} are virtual temperature of the 2-m parcels and the environment as a function of height, $\mathbf{V}_{6\mathrm{km}}$ and $\mathbf{V}_{10\mathrm{m}}$ are horizontal wind vectors at 6 km and 10 m AGL, $\mathbf{V}$ is the horizontal wind vector as a function of height, $\mathbf{C}$ is the storm motion vector following the definition and calculation from Bunkers et al. (2000), $z_b = 10$ m is the altitude of the layer bottom, $z_t = 3$ km is the altitude of the layer top, and $\hat{\mathbf{k}}$ is the vertical unit vector.

To generate climatological distributions of these SLS environmental proxies and parameters over North America, we first use Eqs. (1)–(6) to calculate each for the period 1980–2014 from 3-hourly model outputs. We then calculate their 99th percentiles for each grid point based on their time series during March–August, as SLS environments in general peak in spring and summer (Diffenbaugh et al. 2013; Li et al. 2020; Taszarek et al. 2020). Considering that the specific seasonal phase (peak month) of these environments varies regionally, we also analyze changes in their seasonal cycle using their monthly 99th percentiles for each experiment. Although L20 noted an overestimation of SLS environments over the eastern United States in CTRL, this may not affect their responses in each experiment, as these biases are associated with systematic model biases of temperature and moisture in CAM6 and thus may persist in the experiments.

We also seek to understand how changes in the constituent parameters (ΔCAPE, ΔS06, or ΔSRH03) affect changes in the combined proxies (ΔCAPES06 or ΔEHI03). We decompose fractional changes in CAPES06 according to

$$\frac{\Delta\mathrm{CAPES06}}{\mathrm{CAPES06_{CTRL}}} = \frac{\Delta\mathrm{CAPE}}{\mathrm{CAPE_{CTRL}}} + \frac{\Delta\mathrm{S06}}{\mathrm{S06_{CTRL}}} + \frac{\Delta\mathrm{CAPE}}{\mathrm{CAPE_{CTRL}}} \times \frac{\Delta\mathrm{S06}}{\mathrm{S06_{CTRL}}}, \tag{7}$$

where $\mathrm{CAPE_{CTRL}}$ and $\mathrm{S06_{CTRL}}$ are CAPE and S06 associated with CAPES06 in CTRL ($\mathrm{CAPES06_{CTRL}}$). Delta (Δ) denotes the difference between each experiment and CTRL (i.e., noTOPO or noGOM minus CTRL). The term on the left-hand side of Eq. (7) is the fractional change of CAPES06 in each experiment relative to CTRL. The first and second terms on the right hand side represent the fractional changes due to changes in the associated CAPE and S06, and the third term is a second-order residual term that is generally small. This decomposition method is similar to a statistical framework developed to isolate the dynamic and thermodynamic components of cloud changes (Bony et al. 2004) or extreme precipitation (Emori and Brown 2005; Chen and Chavas 2020). Similarly, the fractional change in EHI03 is given by

$$\frac{\Delta\mathrm{EHI03}}{\mathrm{EHI03_{CTRL}}} = \frac{\Delta\mathrm{CAPE}}{\mathrm{CAPE_{CTRL}}} + \frac{\Delta\mathrm{SRH03}}{\mathrm{SRH03_{CTRL}}} + \frac{\Delta\mathrm{CAPE}}{\mathrm{CAPE_{CTRL}}} \times \frac{\Delta\mathrm{SRH03}}{\mathrm{SRH03_{CTRL}}}. \tag{8}$$

TABLE 1. Identifying criteria for the SLS-relevant synoptic-scale features: southerly GPLLJs, drylines, EMLs, and extratropical cyclone activity defined using both cyclone tracking and 850-hPa EKE. The reader is referred to Li et al. (2020) for detailed explanations.

Synoptic-scale features	Identifying criteria
Southern Great Plains low-level jet (GPLLJ)	1) Maximum wind speed below 3000 m: $V_{max} \geq 10\,m\,s^{-1}$
	2) Largest decrease from V_{max} to wind at 3000 m: $\Delta V \geq 5\,m\,s^{-1}$
	3) Direction of V_{max} falls between 113° and 247°
Dryline	1) Horizontal gradient of surface specific humidity: $\lvert\nabla_H q\rvert \geq 3 \times 10^{-5}\,km^{-1}$ and $\partial q/\partial x > 0$
	2) Surface temperature: $\partial T/\partial x < 0.02\,K\,km^{-1}$
	3) Surface wind direction on the west side is 170°–280° and on the east side 80°–190°
Elevated mixed layer (EML)	1) A layer with lapse rate $\geq 8.0\,K\,km^{-1}$ through a depth of at least 200 hPa
	2) Relative humidity increases from the base to the top of the layer
	3) The base is higher than 1000 m but below 500-hPa level
	4) Average lapse rate between the base and surface $\leq 8.0\,K\,km^{-1}$
Cyclone track	1) Candidate cyclones are SLP minima with a closed contour 2 hPa greater than minima
	2) The closed contour lies within 6 great circle degrees of the minimum
	3) Candidates are stitched together in time by searching within an 8° great circle radius at the next time increment for another candidate cyclone to form a cyclone track
	4) A cyclone track must exist for at least 24 h
850-hPa eddy kinetic energy (EKE)	1) Determine (u', v'), horizontal velocity deviation from annual mean velocities
	2) Apply a 2–6-day Butterworth bandpass filter to (u', v')
	3) EKE = 0.5 $(u'^2 + v'^2)$

2) SLS-RELEVANT SYNOPTIC-SCALE FEATURES

To understand responses of SLS environments, we then analyze changes in key synoptic-scale features associated with the formation of SLS environments over North America: southerly GPLLJs, drylines, EMLs, and extratropical cyclone activity. We follow L20 and references therein to identify GPLLJs (Bonner 1968; Whiteman et al. 1997; Walters et al. 2008; Doubler et al. 2015), drylines (Hoch and Markowski 2005; Duell and Van Den Broeke 2016), EMLs (Banacos and Ekster 2010; Ribeiro and Bosart 2018), and extratropical cyclone activity defined by both explicit cyclone tracking (Ullrich and Zarzycki 2017; Zarzycki 2018) and the 2–6-day Butterworth bandpass filtered eddy kinetic energy (EKE) at 850 hPa (Blackmon 1976; Russell 2006; Ulbrich et al. 2008; Harvey et al. 2014; Schemm and Schneider 2018). Identifying criteria for each are summarized in Table 1; the reader is referred to L20 for detailed explanations. We analyze the responses of mean occurrence frequency of these synoptic-scale features during March–August of 1980–2014 in noTOPO and noGOM relative to CTRL.

3) MEAN STATE AND CHARACTERISTIC SYNOPTIC FLOW PATTERN

To better understand responses of SLS environments and the associated synoptic-scale features, we analyze differences in the mean-state atmosphere for each experiment. We examine changes of low-level moisture and temperature (925 and 850 hPa), which are relevant to the CAPE response. We also examine changes of the horizontal flow fields at lower and upper levels (925, 850, and 250 hPa), which are relevant to the S06 and SRH03 response (Trapp et al. 2007; Diffenbaugh et al. 2013; Agard and Emanuel 2017; Chen et al. 2020; Li et al. 2020). In addition, responses of the mean 925-hPa moisture transport and 850-hPa wind and temperature, especially during warm seasons, may be associated with changes in GPLLJs and EMLs (Pan et al. 2004; Ting and Wang 2006; Ribeiro and Bosart 2018). Meanwhile, responses in the mean 250-hPa wind speed indicate shifts in the jet stream relevant to extratropical cyclone activity (Holton 1973).

Additionally, we evaluate changes in the composite synoptic patterns associated with extreme SLS environments to examine the extent to which mean-state responses are also found in the characteristic synoptic flow responses associated with extreme SLS environments. As past work has identified common synoptic patterns of SLS events and environments over much of the eastern United States (Barnes and Newton 1986; Johns and Doswell 1992; Johns 1993; Mercer et al. 2012; Li et al. 2020), our analysis also examines if these common synoptic patterns are sensitive to the existence of elevated terrain and the Gulf of Mexico. Here we focus on two subregions, R-inland and R-coast, defined in Fig. 2a. Region R-inland represents an inland region over the northern Great Plains where the SLS environments reach a local maximum in CTRL. The associated composite synoptic patterns over R-inland in CTRL are similar to the common synoptic patterns of severe weather events over the Great Plains (Li et al. 2020). Region R-coast represents a coastal region over the southeastern United States where responses of SLS environments in experiments are relatively small (detailed below in the following sections). The associated characteristic synoptic patterns over R-coast in CTRL are known to be different from the common synoptic patterns over the Great Plains (Li et al. 2020). Following L20, we identify an extreme case in a region during March–August when the CAPES06 exceeds its local 99th percentile in at least 80% of the total grid points within the region. Composite synoptic patterns are generated by averaging variable fields from the identified cases. Specifically, we analyze the composite patterns of horizontal wind speed and geopotential height at 250 hPa, temperature and geopotential height at 850 hPa, and

near-surface properties including 925-hPa specific humidity and wind, and sea level pressure.

3. Responses to removing North American topography (noTOPO)

We first analyze responses of SLS environments to the removal of elevated terrain by comparing noTOPO with CTRL. To better understand why these responses occur, we also examine differences in synoptic-scale features (southerly GPLLJs, drylines, EMLs, and extratropical cyclone activity) that are in general favorable to the generation of these environments, as well as examine differences in the mean state and characteristic synoptic patterns.

a. SLS environments

We begin by analyzing responses of extreme values (99th percentiles) of SLS environmental proxies and parameters during March–August in noTOPO (Figs. 3g–l), as compared to CTRL (Figs. 3a–f). Removing elevated terrain strongly reduces CAPES06 and EHI03 over much of the eastern half of the United States, with the reduction extending into south-central and southwestern Canada (Figs. 3g,h). The largest decrease occurs near the local maxima in CTRL over the northern Great Plains and southern Texas for CAPES06 ($\sim -30\,000\ m^3\ s^{-3}$) and in the central Great Plains for EHI03 (~ -4). The reduction along the east coast and the southeastern United States, which may be partly due to the removal of the Appalachian Mountains, is relatively small. CAPE is broadly reduced ($\sim -1000\ J\ kg^{-1}$) over a swath stretching from southwestern Canada across the Great Plains to the southeastern United States, consistent with decreases in CAPES06 and EHI03, whereas it remains similar to CTRL or is slightly enhanced over the south-central United States (Fig. 3i). Removing elevated terrain only slightly increases S06 ($\sim +6\ m\ s^{-1}$) along the U.S.–Canada border east of the Rocky Mountains (Fig. 3j). The modest zonal asymmetry of S06 persists over the continental United States, highlighting how surface thermodynamic variability (land–ocean and SST variability) still generates a stationary wave pattern (Kaspi and Schneider 2013). Removing elevated terrain causes SRH03 to become substantially more zonally symmetric, especially over the Great Plains (Fig. 3k). SRH03 decreases over the eastern half of the United States with strongest reductions ($\sim -200\ m^2\ s^{-2}$) over the central Great Plains. Finally, removing elevated terrain strongly reduces CIN over the Great Plains with the peak reduction over the northern Great Plains (Fig. 3l); the response pattern is similar to CAPES06 and EHI03 and broadly consistent with reductions in CAPE.

SLS environments exhibit a strong seasonal cycle, and the responses of extreme CAPES06 and EHI03 occur principally in the warm seasons and hence reduce their seasonal cycle magnitudes (Figs. 4a,b). The seasonal response of CAPES06 is predominantly tied to CAPE, as the response of S06 is consistently small throughout the year with a slight decrease in summer and a slight increase in winter and spring (Figs. 4c,d). The seasonal response of EHI03 is tied to both CAPE and SRH03, as both are strongly reduced in the warm seasons (Figs. 4b,c,e). A similar dampening of the seasonal cycle is also found in the response of CIN (Fig. 4f).

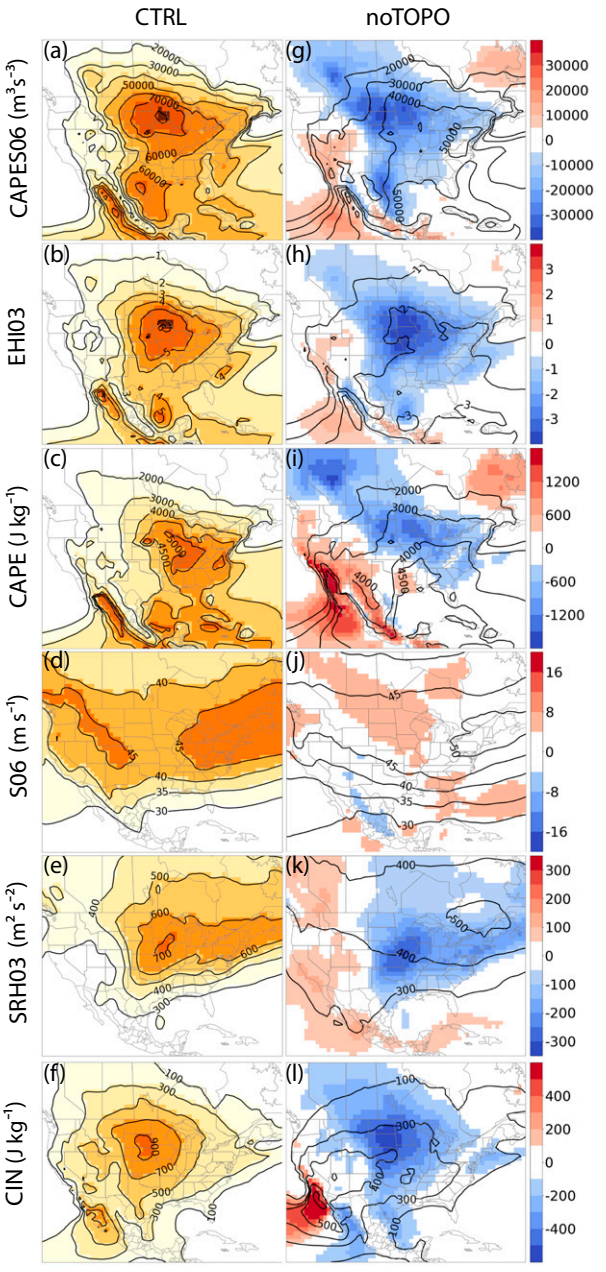

FIG. 3. (a)–(f) CTRL 99th percentiles (contour lines + filled contours) of CAPES06, EHI03, CAPE, S06, SRH03, and CIN. (g)–(l) As in (a)–(f), but for noTOPO 99th percentiles (contour lines) and responses (noTOPO minus CTRL; filled contours). The 99th percentiles are generated at each grid point from the 3-hourly full period (1980–2014) during March–August.

In addition to the magnitude of seasonal cycle, the spatial distribution of the seasonal phase (peak month) of these environments is also modified (Figs. 4g–r). In CTRL, the seasonal cycles of CAPES06 and EHI03 both peak in April/May near the Gulf Coast and then progresses inland toward the continental interior through July; this progression is confined zonally to the region downstream of the Rockies over the Great Plains.

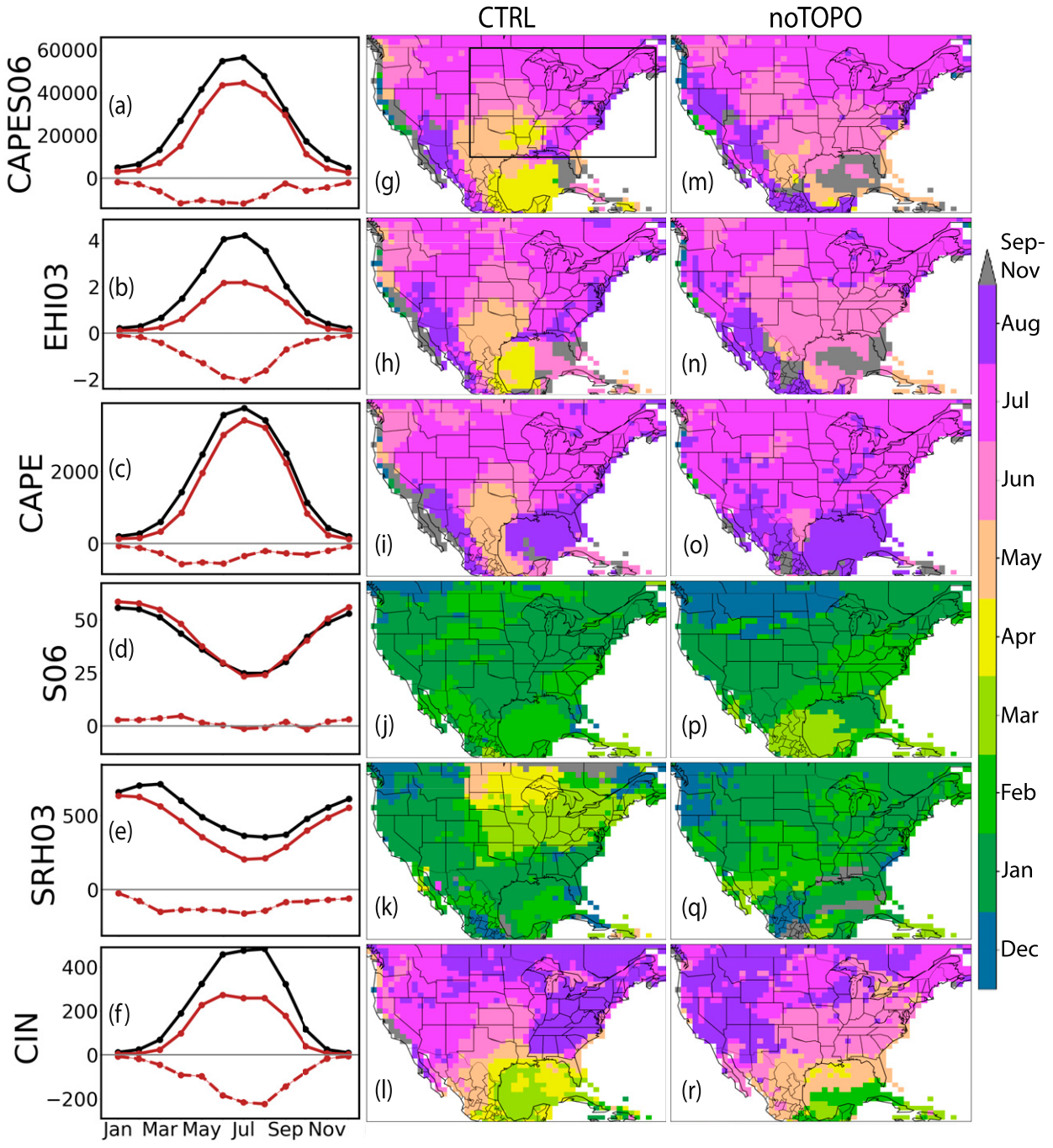

FIG. 4. (a)–(f) The monthly 99th percentiles of CAPES06, EHI03, CAPE, S06, SRH03, and CIN for CTRL (black solid line) and noTOPO (red solid line), and differences in noTOPO relative to CTRL (red dashed line), averaged for land grid points over the eastern half of the United States [within the black box in (g)]. (g)–(l) Peak month with the maximum monthly 99th percentiles of each parameter for CTRL; (m)–(r) as in (g)–(l), but for noTOPO.

Removing elevated terrain causes CAPES06 and EHI03 to peak in June over the entire southern Great Plains and southeastern United States (Figs. 4m,n). This peak is 1–2 months later than CTRL over the southern Great Plains but 1–2 months earlier over the southeastern United States (Figs. 4m,n vs Figs. 4g,h). Hence, elevated terrain appears responsible for the zonal variability in the seasonality of SLS environments over the southeastern United States in the real world. This response is tied to CAPE, which exhibits a similar pattern in its response particularly over the southern Great Plains, with the peak month

shifting from late spring (May–June in CTRL; Fig. 4i) to late summer (July–August in noTOPO; Fig. 4o); the seasonal peak in CAPE becomes zonally symmetric, occurring in July north of ~31°N and August to the south. In contrast, the peak month of S06 changes only minimally, occurring in winter (December–February; Fig. 4p) similar to CTRL (Fig. 4j). SRH03 is phase shifted strongly, from spring (March–May in CTRL; Fig. 4k) to winter (January–February in noTOPO; Fig. 4q) over much of the eastern half of North America, especially over the northern Great Plains and southern Canada. This suggests the weakened influence of the reduced GPLLJs in spring in noTOPO (detailed below). As a result, the seasonal phase of SRH03 becomes more similar to that of S06 driven predominantly by the jet stream. Finally, the peak month of CIN over the eastern third of the United States shifts from late summer (August in CTRL; Fig. 4l) to early summer (June in noTOPO; Fig. 4r), rendering the seasonal peak in CIN more zonally symmetric east of the Rocky Mountains, similar to CAPE, while still retaining significant meridional variability. Overall, removing elevated terrain suppresses the inland progression of the seasonal cycle of SLS environments and leads to relatively uniform seasonal phase over the eastern United States.

Finally, we explicitly attribute the fractional changes in each combined proxy (CAPES06 or EHI03) to changes in their constituent parameters (CAPE, S06, or SRH03) using Eqs. (7) and (8). We quantify the responses in the center of mass of extreme CAPES06 or EHI03 and the extent to which these responses are due to changes in the CAPE, S06, or SRH03. The center of mass is defined by the product of median CAPE and S06 or SRH03 associated with extreme values (defined by the top 1% cases) of CAPES06 or EHI03. In noTOPO, the relative contributions to decreases in extreme CAPES06 due to changes in CAPE and S06 varies across regions though both parameters are important (Figs. 5a–d). Over the northern Great Plains and much of the eastern third of the United States, the decrease (~−40%) is driven more by a decrease in CAPE (from −20% to −40%) than S06 (~−20%). Over the southern Great Plains, the decrease (from −20% to −40%) is driven primarily by a decrease in S06 (from −20% to −40%). Decreases in extreme EHI03 are broadly similar to decreases in extreme CAPES06, although this response is driven more strongly by decreases in SRH03 rather than CAPE over much of the eastern half of the United States (Figs. 5e–h). Hence, while the combined proxies appear to decrease broadly over eastern North America, the underlying reasons for their decrease actually vary regionally.

b. *SLS-relevant synoptic-scale features*

The substantial reduction of SLS environments described above is closely aligned with the responses of key synoptic-scale features commonly associated with SLS environments over North America. Southerly GPLLJs, drylines, EMLs, and extratropical cyclone activity are all strongly reduced during March–August (Fig. 6), likely contributing to the reduction of CAPE, S06 or/and SRH03 in noTOPO.

Specifically, removing elevated terrain substantially reduces GPLLJs (Figs. 6a,e), especially over the southern Great Plains.

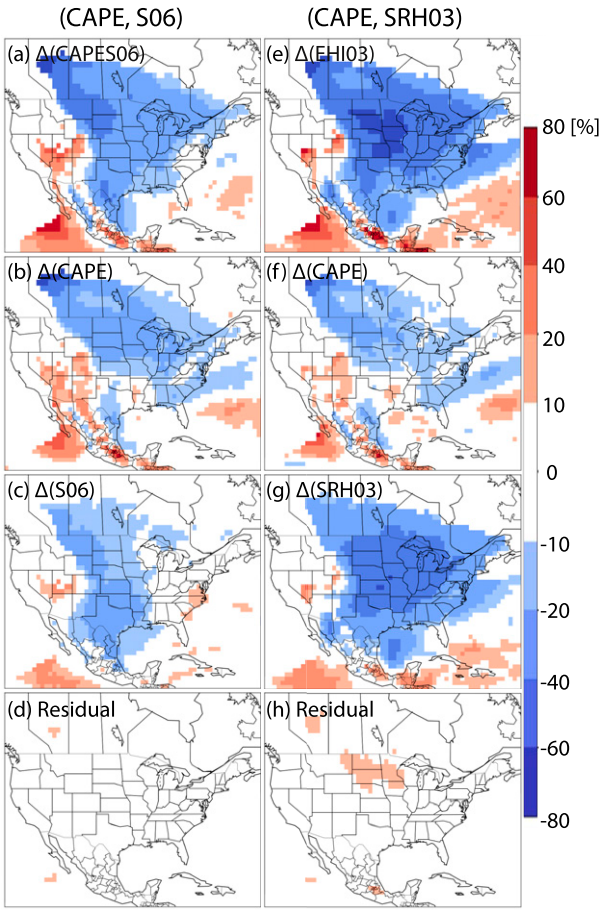

FIG. 5. The noTOPO percentage changes (as compared to CTRL) in (a) the center of mass of the top 1% cases of CAPES06 during March–August of 1980–2014 for each grid point, and the associated (b) median CAPE, (c) median S06, and (d) the residual of the top 1% cases of CAPES06, corresponding to each term in Eq. (7). Center of mass of the top 1% cases of CAPES06 is represented by the product of the associated median CAPE and median S06. (e)–(h) As in (a)–(d), but for percentage changes in the center of the top 1% cases of EHI03 and the associated terms, corresponding to Eq. (8).

This response is qualitatively similar to past work (Pan et al. 2004; Ting and Wang 2006). GPLLJs are not entirely eliminated by removing elevated terrain, however, as a local frequency maximum is still retained over northeastern Mexico (Fig. 6e). Hence, upstream elevated terrain indeed appears essential to the production of GPLLJs, although land–ocean thermal contrast may also play a small role (Parish 2000). The reduced occurrence of GPLLJs indicates weakened mean low-level meridional winds, which thus contributes to the slight weakening of S06 in summer and the strong weakening of SRH03 in spring and summer. Moreover, it may correspond to reduced northward moisture transport into the continental interior, which may partially explain the broad reduction of CAPE in noTOPO; this topic is examined further below.

Removing elevated terrain effectively eliminates drylines (Figs. 6b,f). This implies a weakening of horizontal near-surface moisture gradients and moisture convergence over the Great Plains. This outcome reflects both the enhanced

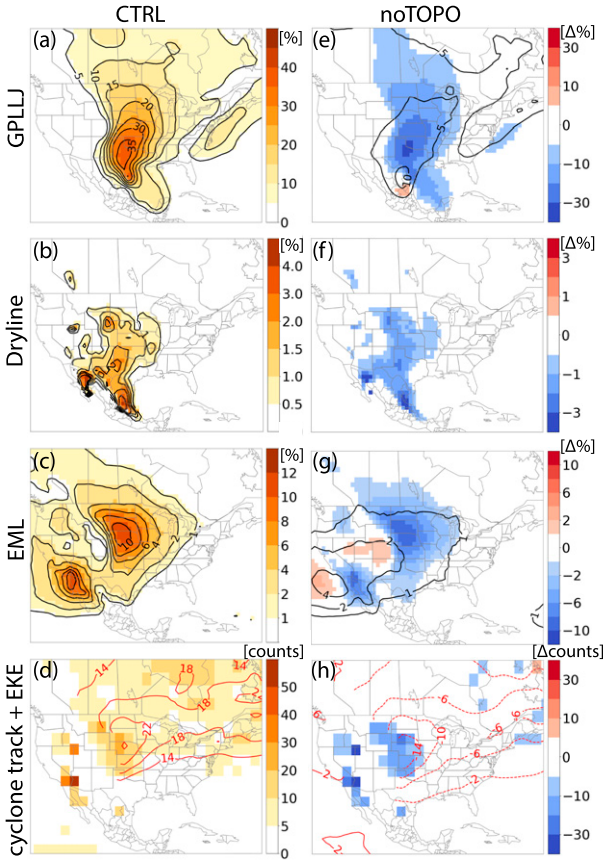

FIG. 6. (a)–(c) CTRL percentage frequency (contour lines + filled contours) of southerly GPLLJs, drylines, and EMLs during March–August of 1980–2014. (d) CTRL mean frequency of cyclone track density based on sea level pressure field (counts per 2.5° × 2.5° grid box; filled contours) and mean 2–6-day Butterworth bandpass filtered EKE at 850 hPa ($m^2 s^{-2}$; contour lines) during March–August of 1980–2014. (e)–(g) As in (a)–(c), but for noTOPO percentage frequency (contour lines) and the response (noTOPO percentages minus CTRL percentages; filled contours). (h) As in (d), but for noTOPO responses only. Detailed detection criteria for each synoptic-scale feature are listed in Table 1.

surface moisture to the west by the reduced elevation and the decreased surface moisture over the Great Plains by the weakened northward transport of moisture from the Gulf of Mexico.

Removing elevated terrain strongly reduces the frequency of EMLs over the Great Plains, but does not eliminate them (Figs. 6c,g). Though perhaps unsurprising, these results confirm that the elevated terrain to the west is indeed essential to the generation of EMLs east of these mountains (Carlson et al. 1983). Since the presence of an EML and the associated capping inversion permit the build-up of CAPE in an atmospheric column by inhibiting convective initiation (Carlson et al. 1983; Farrell and Carlson 1989; Banacos and Ekster 2010; Ribeiro and Bosart 2018), this reduction of EMLs is fully consistent with the reduction of CAPE and CIN found above.

Finally, removing elevated terrain also reduces extratropical cyclone activity substantially, especially on the lee of the Rocky Mountains over the central United States where the local maximum of cyclone track and 850-hPa EKE is almost eliminated (Figs. 6d,h). These results indicate the key role of the Rocky Mountains in generating stationary waves and thus localizing extratropical cyclone activity over east-central North America, in line with past studies (Broccoli and Manabe 1992; Inatsu et al. 2002; Brayshaw et al. 2009). Given the east-northeastward storm track (Fig. 6d) (Reitan 1974; Zishka and Smith 1980), a reduction of cyclogenesis on the lee of the Rocky Mountains further reduces cyclone activity over the Great Lakes and off the northeastern U.S. coast (Fig. 6h). Fewer extratropical cyclones also likely contribute to the inland reduction in CAPE due to the weakened low-level moisture and heat convergence associated with the warm sectors of extratropical cyclones (Hamill et al. 2005; Tochimoto and Niino 2015). Moreover, their absence will also reduce S06 and SRH03 typically generated by the cyclonic circulation and associated with these baroclinic systems (Doswell and Bosart 2001). Note though that removing elevated terrain has a weaker influence on tracked cyclone activity over higher latitudes in Canada where the jet stream remains relatively zonal.

c. *Mean state and characteristic synoptic flow pattern*

To further understand these responses of SLS environments, we analyze responses in the mean synoptic patterns at lower and upper levels in noTOPO (Fig. 7). Removing elevated terrain substantially dries and cools the troposphere over much of the eastern half of the United States, especially at low to midlevels in spring and summer (Figs. 7a–h). This response is consistent with the strong reduction of CAPE and the associated synoptic-scale features. Specifically, the drying response throughout the regions, especially over the Great Plains, is associated with the strong weakening in southerly winds at 925 hPa (and 850 hPa) and hence the reduced GPLLJs, which substantially reduces northward moisture transport from the Gulf of Mexico (Figs. 7a–d). Meanwhile, the Great Plains exhibit a strong cooling at 850 hPa that is consistent with the strong reduction of EMLs and hence of CAPE and CIN (Figs. 7e–h). This cooling response weakens moving upward (not shown), and thus reduces midlevel lapse rates, indicative of the CAPE reduction as well. The horizontal flow becomes more zonal at all levels; the substantially weakened low-level meridional winds in spring and summer and the slightly weakened upper-level jet streams in summer (Fig. 7j) are consistent with the reductions of S06 and SRH03 in warm seasons. Note that the mean upper-level jet streams are enhanced in winter and spring over much of the northern half of the United States (Fig. 7l), which likely contributes to the enhanced S06 during these months over this region.

These responses in the mean-state flow are also found in the composite synoptic pattern associated with extreme SLS environments (Fig. 8). Overall, the composite flow pattern is similar without topography in the inland region (R-inland) (Fig. 8a), whereas it differs markedly for the coastal region (R-coast) (Fig. 8b). For R-inland, the region is located downstream of a trough at all levels that advects warm and moist air northward into the continental interior with an upper-level jet maximum to the west in each. The primary difference is the

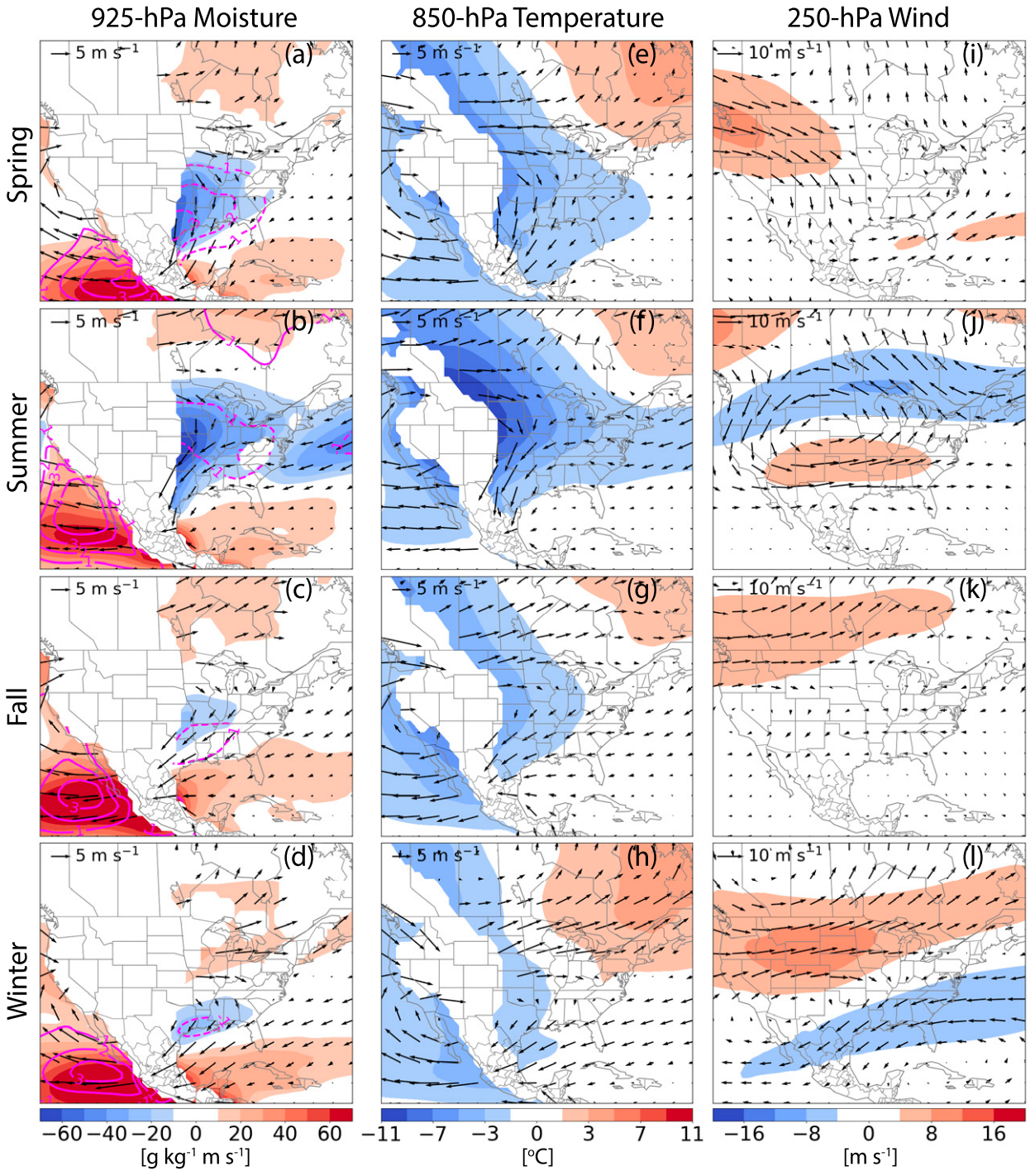

FIG. 7. Responses of mean state in noTOPO (noTOPO minus CTRL) for each season (top–bottom: spring–winter). (a)–(d) Specific humidity (g kg^{-1}; contour lines), wind vector (arrows), and horizontal moisture transport (filled contours) at 925 hPa. (e)–(h) Air temperature (filled contours) and wind vector (arrows) at 850 hPa. (i)–(l) Wind speed (filled contours) and wind vector (arrows) at 250 hPa.

weakened warm advection from the upstream elevated terrain at 850 hPa and the weakened southerly winds and moisture advection from the Gulf of Mexico at 925 hPa, associated with a weaker surface cyclone in noTOPO; this indicates that the cooling and drying response in the mean state atmosphere discussed above persists in composite synoptic patterns. For R-coast, the low-level pattern of warm and moist advection remains in noTOPO (Fig. 8b), but at mid and upper levels a deep trough exists upstream, which differs markedly from the ridge pattern found in CTRL particularly at 250 hPa. Hence,

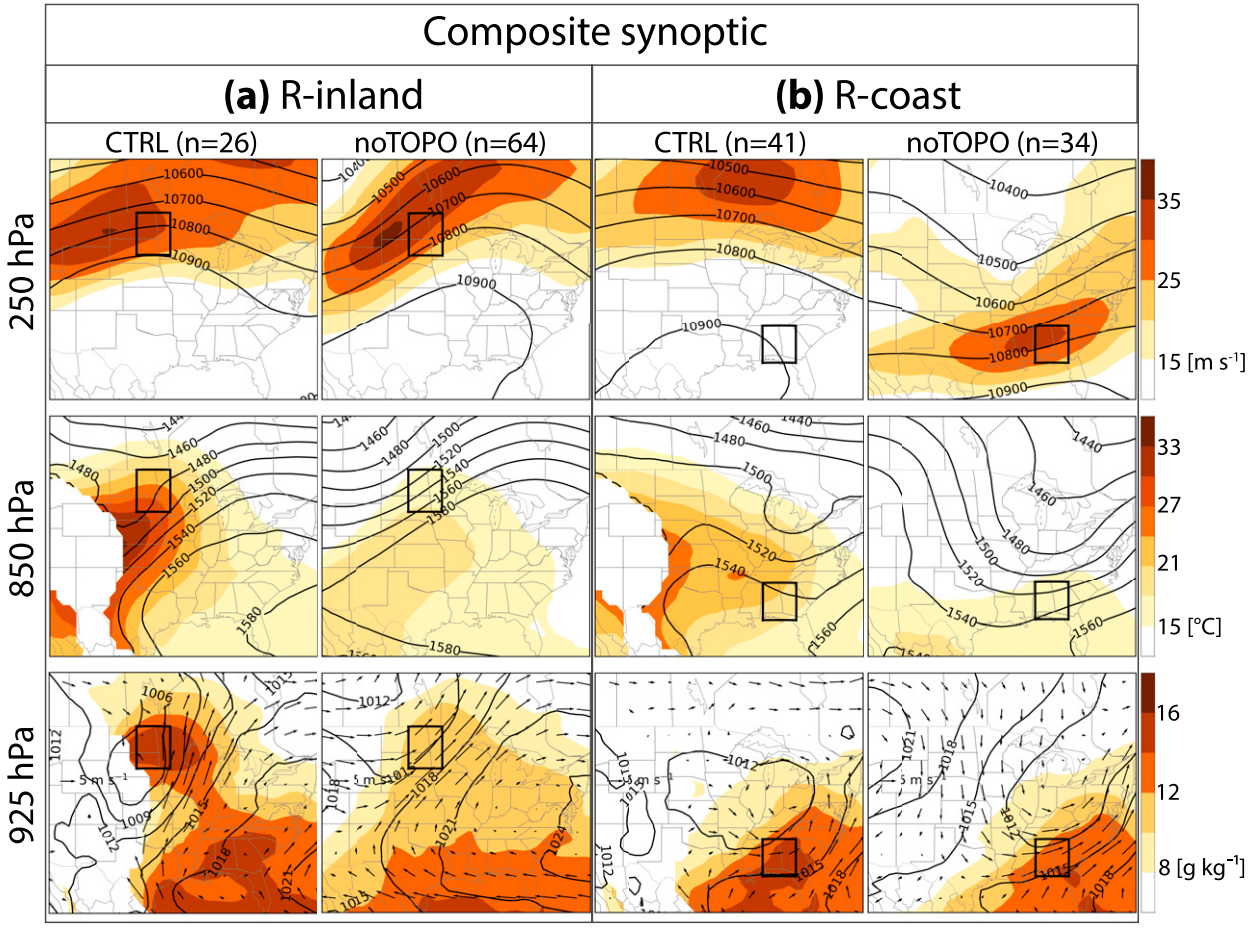

FIG. 8. Composite synoptic patterns for cases associated with extreme SLS environments during March–August of 1980–2014 in (a) R-inland and (b) R-coast, for (left) CTRL and (right) noTOPO. Black squares indicate the location of subregions. (top) 250-hPa wind speed (filled contours) and geopotential height (m; contour lines). (middle) 850-hPa temperature (filled contours) and geopotential height (m; contour lines). (bottom) 925-hPa specific humidity (filled contours), wind vector (arrows), and sea level pressure (hPa; contour lines).

without elevated terrain, the characteristic synoptic flow pattern is qualitatively similar between the continental interior and near the southeast coast, whereas they are qualitatively different in CTRL. Additionally, we examined these responses in a region over the southern Great Plains (R-SGP), which is at the same longitude as R-inland and the same latitude as R-coast (Figs. S2a,b). The response of R-SGP is similar to R-inland and hence distinct from R-coast, which indicates that latitude alone is not the determining factor; instead, it is a contrast between the inland Great Plains and the coastal Southeast. This may be relevant to the reduced predictability of SLS activity in the Southeast (Miller and Mote 2017).

4. Responses to filling in the Gulf of Mexico (noGOM)

Following the structure of section 3, we next analyze responses to the removal of the Gulf of Mexico by comparing noGOM with CTRL.

a. SLS environments

In contrast to noTOPO, replacing the Gulf of Mexico with land does not strongly change the overall amplitude of extreme CAPES06 and EHI03 relative to CTRL, although it does induce changes in the spatial pattern (Figs. 9a,b,g,h). The primary local maximum shifts southeastward to the Midwest centered over Illinois. This shift emerges due to the reduction of SLS environments over the northern Great Plains (CAPES06: $-10\,000\ \mathrm{m^3\,s^{-3}}$; EHI03: -1) and the enhancement over the eastern third of the United States (CAPES06: $+10\,000\ \mathrm{m^3\,s^{-3}}$; EHI03: $+1$). Meanwhile, the secondary local maximum over southern Texas is eliminated, as CAPES06 and EHI03 are substantially reduced over the region in noGOM ($-20\,000\ \mathrm{m^3\,s^{-3}}$ and -1.5). For constituent parameters, CAPE decreases ($\sim -600\ \mathrm{J\,kg^{-1}}$) over the Great Plains (Figs. 9c,i), whereas S06 and SRH03 change only minimally (Figs. 9d,e,j,k). SRH03 is slightly enhanced ($\sim +100\ \mathrm{m^2\,s^{-2}}$) over the south-central United States. Finally, CIN is enhanced over the Gulf of Mexico itself and much of the eastern half of the United States extending inland from the Gulf of Mexico (Figs. 9f,l). Note that CAPE changes relatively little in this region, a behavior consistent with drier and warmer boundary layer air at roughly fixed moist static energy in this region (Fig. S3), which will increase CIN while keeping CAPE relatively constant

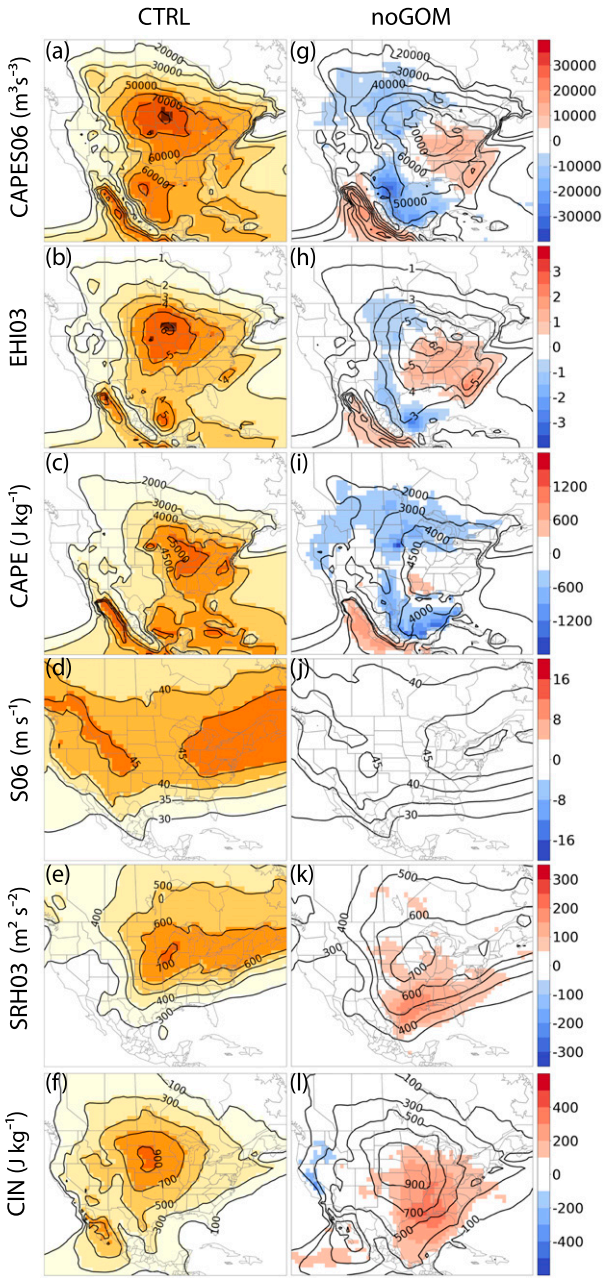

FIG. 9. CTRL vs noGOM for the 99th percentiles of CAPES06, EHI03, CAPE, S06, SRH03, and CIN during March–August of 1980–2014. Plot aesthetics as in Fig. 3.

(Agard and Emanuel 2017; Chen et al. 2020; Chavas and Dawson 2020; Taszarek et al. 2021b).

These responses are consistent throughout the year and thus the amplitudes of their seasonal cycles remain relatively constant (Figs. 10a–f). Nonetheless, replacing the Gulf of Mexico with land does indeed slightly reduce CAPE and increase S06 and SRH03 in spring and summer (Figs. 10c–e). These responses offset each other in the seasonal cycle of CAPES06 and EHI03, resulting in minimal changes in each (Figs. 10a,b). The only exception is CIN, whose seasonal cycle amplitude is enhanced due to increases in the warm seasons (Fig. 10f).

In terms of their seasonal phase, replacing the Gulf of Mexico with land causes seasonal phase shifts primarily over the southeastern United States, as well as over the Gulf of Mexico region itself (Figs. 10g–r). Specifically, CAPES06 and EHI03 peak 2–3 months earlier over the southeastern United States, shifting from July or August in CTRL to May in noGOM (Figs. 10g,h,m,n). The peak month of CAPE remains broadly similar to CTRL (Figs. 10i,o), although it peaks earlier over the Gulf of Mexico (May in noGOM; August in CTRL). Meanwhile, the peak month in S06 shifts slightly earlier over the southeastern United States and the Gulf of Mexico from February to January, whereas SRH03 over the Gulf coast shifts slightly later to February or March from January (Figs. 10j,k,p,q). Finally, CIN peaks 1 month earlier over the southeastern United States, shifting from August in CTRL to July in noGOM (Figs. 10l,r). Overall, replacing the Gulf of Mexico with land extends the inland progression of the seasonal cycle over the Great Plains farther east into the southeastern United States, thereby reducing (though not eliminating) zonal variability in the seasonal cycle, similar to noTOPO.

Finally, we explicitly attribute the changes in each combined proxy (CAPES06 or EHI03) to changes in their constituent parameters (CAPE, S06, or SRH03) using Eqs. (7) and (8) (Fig. 11). In noGOM, CAPES06 and EHI03 change more subtly and nonuniformly in space than in noTOPO. Specifically, the decrease of CAPES06 and EHI03 over the northern Great Plains is driven predominantly by a decrease in CAPE, while their increase over much of the eastern United States is primarily driven by an increase in S06 and SRH03. In combination, the result is an eastward shift of the primary local maximum of CAPES06 and EHI03. Meanwhile, the removal of the secondary local maximum of CAPES06 and EHI03 over southern Texas is driven by decreases in both CAPE and S06 (and SRH03), though CAPE contributes a larger portion.

b. SLS-relevant synoptic-scale features

These SLS environmental responses in noGOM are again consistent with the muted responses of the associated synoptic-scale drivers over North America, as the southerly GPLLJs, drylines, EMLs, and extratropical cyclone activity all change minimally in spring and summer (Fig. 12).

Specifically, replacing the Gulf of Mexico with land has little influence on the frequency of GPLLJs, which is maximized over the southern Great Plains (Figs. 12a,e). Yet the presence of the new land still acts to reduce the local moisture supply at low levels over the Gulf of Mexico, and thus potentially reduces northward moisture transport into the Great Plains. This may contribute to the reduction of CAPE over the Great Plains in noGOM found above. In addition, noGOM does produce an increase in GPLLJs over the Gulf of Mexico and the deep Southeast (Fig. 12e), which are likely a combination of topographically forced (mainly the Mexican Plateau) GPLLJs and coastal GPLLJs due to the enhanced land–ocean thermal contrast between the new land and tropical ocean (Parish 2000). The increased frequency of GPLLJs indicates enhanced mean low-level winds, which may explain the enhanced S06

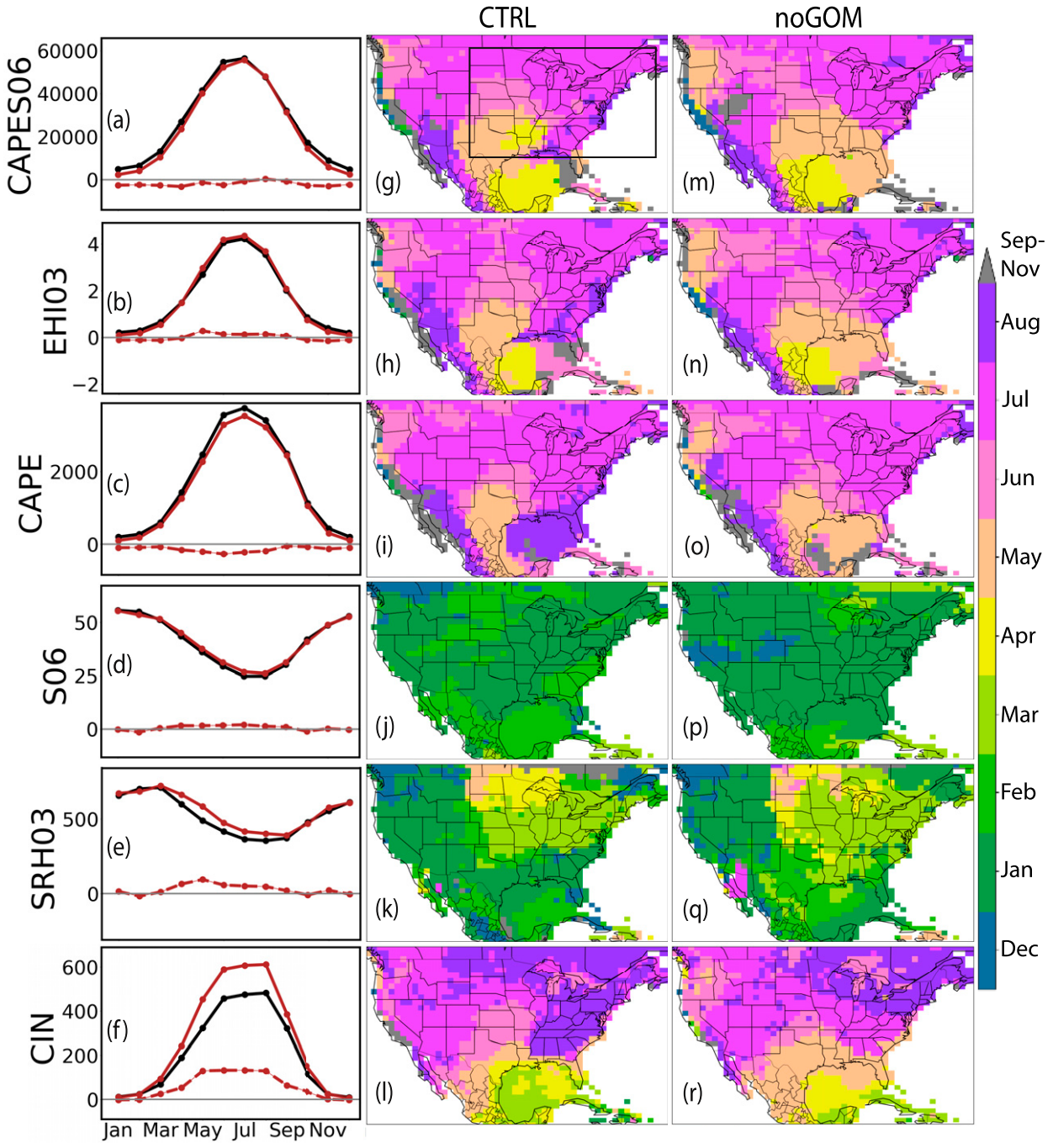

FIG. 10. CTRL vs noGOM for seasonal cycles of extreme CAPES06, EHI03, CAPE, S06, SRH03, and CIN. Plot aesthetics as in Fig. 4.

and SRH03 associated with CAPES06 and EHI03 over much of the eastern third of the United States.

Replacing the Gulf of Mexico with land strongly reduces the frequency of drylines over the northeastern Mexico and western half of Texas, consistent with the local reduction in CAPE, while it has little influence on drylines over the central United States (Figs. 12b,f). These reduced drylines primarily form in spring, while the residual drylines occur mainly in summer (not shown). These results indicate that the Gulf of Mexico is an essential source of moisture for the southern Great Plains in spring, which enhances dryline formations. In contrast, in summer other sources of moisture (e.g., soil and vegetation) likely contribute strongly to dryline formation, in line with findings of Molina and Allen (2019).

Replacing the Gulf of Mexico with land produces slightly more EMLs over the central United States (Figs. 12c,g). Considering

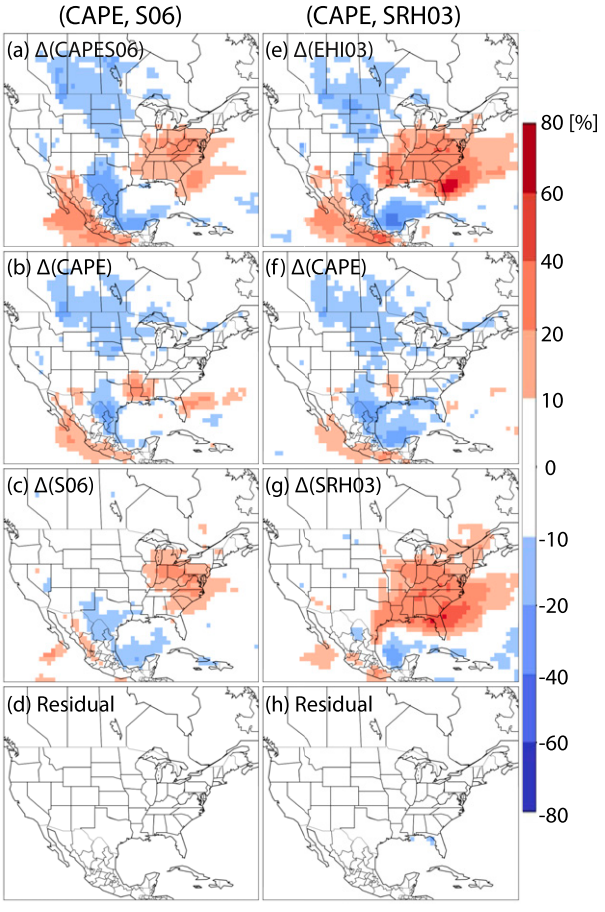

FIG. 11. Attributions of responses in noGOM extreme CAPES06 and EHI03. Plot aesthetics as in Fig. 5.

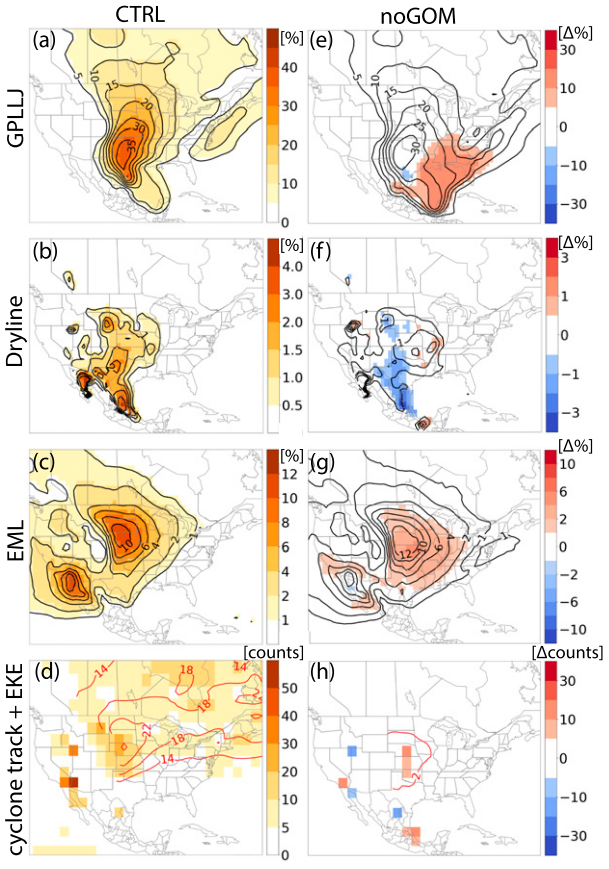

FIG. 12. CTRL vs noGOM for the March–August frequency of southerly GPLLJs, drylines, EMLs, and extratropical cyclone activity. Plot aesthetics as in Fig. 6.

that the horizontal advection of elevated air masses with steep lapse rates dominates the formation and maintenance of EMLs over North America (Banacos and Ekster 2010; Ribeiro and Bosart 2018), the increase in EMLs is in part consistent with the enhanced CIN, though it does not necessarily increase CAPE.

Finally, replacing the Gulf of Mexico with land has little influence on extratropical cyclone activity. The cyclone track frequency and 850-hPa EKE in noGOM are broadly similar to CTRL, though with a slight increase over a small region in the central Great Plains (Figs. 12d,h).

c. *Mean state and characteristic synoptic flow pattern*

Finally, to further understand the responses of SLS environments, we analyze responses in the mean synoptic patterns at lower and upper levels in noGOM (Fig. 13). Replacing the Gulf of Mexico with land principally causes the mean-state response to dry and warm at low levels, although in the far southeastern United States it is slightly moistened. This dry and warm response is strongest over the Gulf of Mexico region itself and southern Texas (Figs. 13a–h), due to the reduced surface moisture supply from the new land and its lower heat capacity as compared to ocean water. These responses over the Gulf of Mexico strongly affect the southern Great Plains via inland advection of this drier and warmer air by the large-scale flow. While the enhanced 850-hPa temperature in spring and summer over the southern Great Plains ($\sim+3$ K) may actually contribute to the modest increase in the frequency of EMLs over the Great Plains noted above, which could translate to higher CAPE in isolation, this effect is offset by the low-level drying response ($\sim-2\,\mathrm{g\,kg^{-1}}$), resulting in a decrease in CAPE; this is further supported by the reduction of low-level moist static energy over the Great Plains (Fig. S3).

Ultimately, this lower-tropospheric drying and warming effect moves farther inland toward the continental interior although it weakens in magnitude (Figs. 13a–h). Meanwhile, there is a slight enhancement of moisture transport at 925 hPa in spring and summer over the eastern Gulf coast (Figs. 13a,b), possibly due to the strengthened southerly winds (and hence the increased GPLLJs) enhancing moisture transport from the remote tropical ocean. Analysis of changes in the associated moisture budget could quantify this effect (Molina and Allen 2019, 2020) in future work. Although the drying effect dominates the reduced CAPE over the Great Plains, the warming response itself does indeed increase low-level dry static energy over much of the eastern United States, and thus contributes to the enhanced CIN found

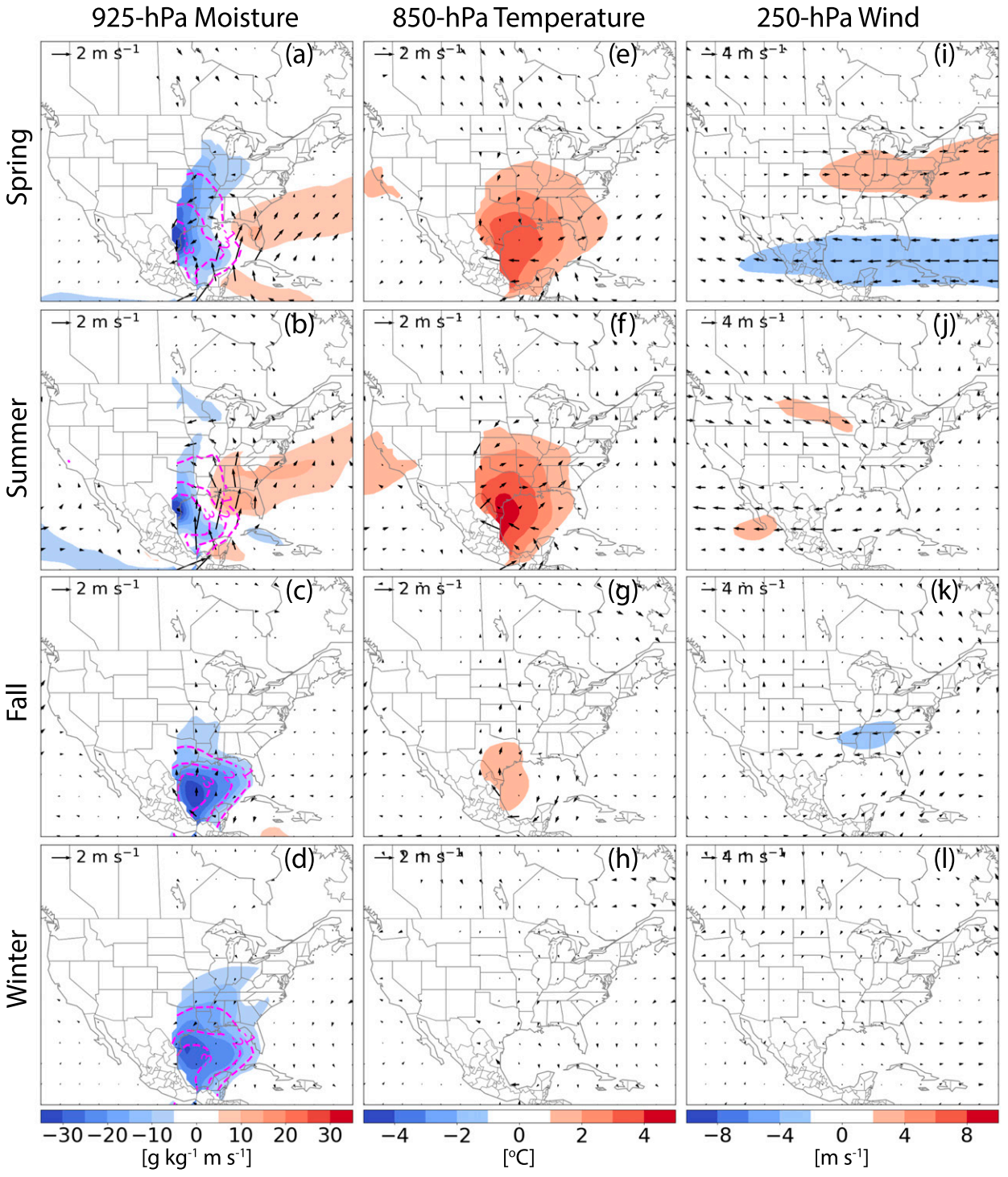

FIG. 13. The noGOM responses of the seasonal mean state at 925, 850, and 250 hPa. Plot aesthetics as in Fig. 7.

above. In addition, the inland flow remains strong in spring and summer when persistent low-level southerly winds are present (Figs. 13a–d). These southerly winds are enhanced over the deep south, especially in summer, consistent with the increased GPLLJs noted above. This flow response is also consistent with the enhanced S06 and SRH03 associated with CAPES06 and EHI03 over much of the eastern third of the United States. The upper tropospheric flow in noGOM is broadly similar to CTRL (Figs. 13i–l), indicating that the mean-state response to filling the Gulf of Mexico is confined primarily to the lower troposphere.

The composite synoptic patterns of extreme SLS environments have relatively small differences between noGOM and CTRL in both regions R-inland and R-coast (Figs. 14a,b). The 850-hPa temperature increases slightly in noGOM (Figs. 14a,b), indicative of the low-level warming effects from removing the Gulf of Mexico as was found in the mean-state response. The 925-hPa moisture and flow fields do not change strongly in noGOM, indicating that local moisture sources (e.g., soil and vegetation) or far-field sources from the tropical oceans are more important for the formation of extreme SLS environments over the continental interior and the southeastern United States, in line with Molina and Allen (2019). A slight difference is found for the region R-SGP over the southern Great Plains, where the composite low-level moisture is reduced due to the reduced moisture transport from the filled Gulf of Mexico though the inland winds remain strong (Figs. S2a,c); these are consistent with the mean-state responses discussed above. Overall, in contrast to responses in noTOPO, replacing the Gulf of Mexico does not strongly impact differences in the composite synoptic between inland and coast. Hence, it confirms that the regional variability in characteristic synoptic flow patterns between the Great Plains and the southeastern United States primarily depends on the upstream elevated terrain rather than the Gulf of Mexico.

5. Conclusions

The eastern half of the United States is one of the principal hot spots for SLS activity globally. The prevailing conceptual model for this behavior, proposed by Carlson et al. (1983), posits that elevated terrain to the west and the Gulf of Mexico to the south together are critical to produce environments conducive to SLS activity. We tested this conceptual model in the CAM6 global climate model by conducting two experiments relative to an AMIP-style control run (CTRL): 1) North American topography removed (noTOPO) and 2) the Gulf of Mexico converted to land (noGOM). We focused our analysis on responses of SLS environments during warm seasons, defined by extreme values (99th percentiles) of two common SLS environmental proxies (CAPES06 and EHI03) during March–August, and we quantitatively attributed their changes to changes in their constituent parameters (CAPE, S06, and SRH03). To better understand these responses, we next analyzed responses of a set of key synoptic-scale features commonly associated with the generation of SLS environments: southerly GPLLJs, drylines, EMLs, and extratropical cyclone activity. Finally, we analyzed changes in the mean state and characteristic synoptic flow patterns to understand how these responses are related to changes in the large-scale circulation.

We summarize our primary results as follows:

1) The existence of SLS environments over North America does depend strongly on upstream elevated terrain (noTOPO vs CTRL).
   (i) Removing elevated terrain substantially reduces extreme CAPES06 and EHI03 over North America, particularly over the northern Great Plains, leaving a residual distribution that is maximized near the Gulf coast and decays moving inland toward the continental interior. Their reduction is driven by the reduction of all three constituent parameters (CAPE, S06, and SRH03), although their contributions vary spatially. The response of these SLS proxies occurs largely during peak SLS seasons in spring and summer, and thus reduces the amplitude of their seasonal cycles. Moreover, removing elevated terrain suppresses the inland progression of the SLS seasonal cycle and produces a relatively uniform seasonal phase that peaks in June over the southern United States and July over the northern United States.
   (ii) This response is accompanied by a strong reduction in the occurrence of all key SLS-relevant synoptic-scale features. The reduced EMLs indicate the weakened downstream advection of warm well-mixed layers with steep lapse rates from the elevated terrain, consistent with the cooling of the 850-hPa mean state, especially over the Great Plains. The reduced GPLLJs and extratropical cyclones are consistent with reduced inland low-level moisture transport from the Gulf of Mexico which dries the lower troposphere, as well as a more zonal tropospheric mean flow. Thus, taken together, the cooler and drier mean-state atmosphere with weakened low-level inland winds is less favorable to the generation of CAPE, S06, and SRH03, and hence the formation of SLS environments, despite the reduction in CIN. The characteristic synoptic flow pattern associated with SLS environments near the Gulf coast differs markedly from the upstream trough pattern found inland in CTRL, but it becomes similar when elevated terrain is removed, indicating that elevated terrain generates spatial variability in how SLS environments are produced by the large-scale flow.
2) The existence of SLS environments over North America depends much less strongly on the Gulf of Mexico though its effects are not negligible (noGOM vs CTRL).
   (i) Replacing the Gulf of Mexico with land shifts the primary local maximum of extreme CAPES06 and EHI03 southeastward from the northern Great Plains into the southern Midwest, primarily driven by a reduction of CAPE over the northern Great Plains and an increase in S06 and SRH03 over the eastern third of the United States. It further eliminates the secondary smaller local maximum over the southern Great Plains, primarily driven by the reduction of CAPE. The amplitude of the seasonal cycle is not strongly influenced, though its spatial footprint expands eastward, with its peak over the southeastern United States shifting 1–2 months earlier to May similar to the southern Great Plains.
   (ii) Consistent with modest responses in SLS environments, there are modest changes in the key SLS-relevant synoptic-scale features. Drylines are reduced in spring, consistent with the drying of the 925-hPa mean state, resulting in a decrease in CAPE over the Great Plains. The more frequent EMLs are consistent with the strong warming of the 850-hPa mean state, which may contribute to the increase in CIN though it does not necessarily translate to increasing CAPE. This lower tropospheric drying and

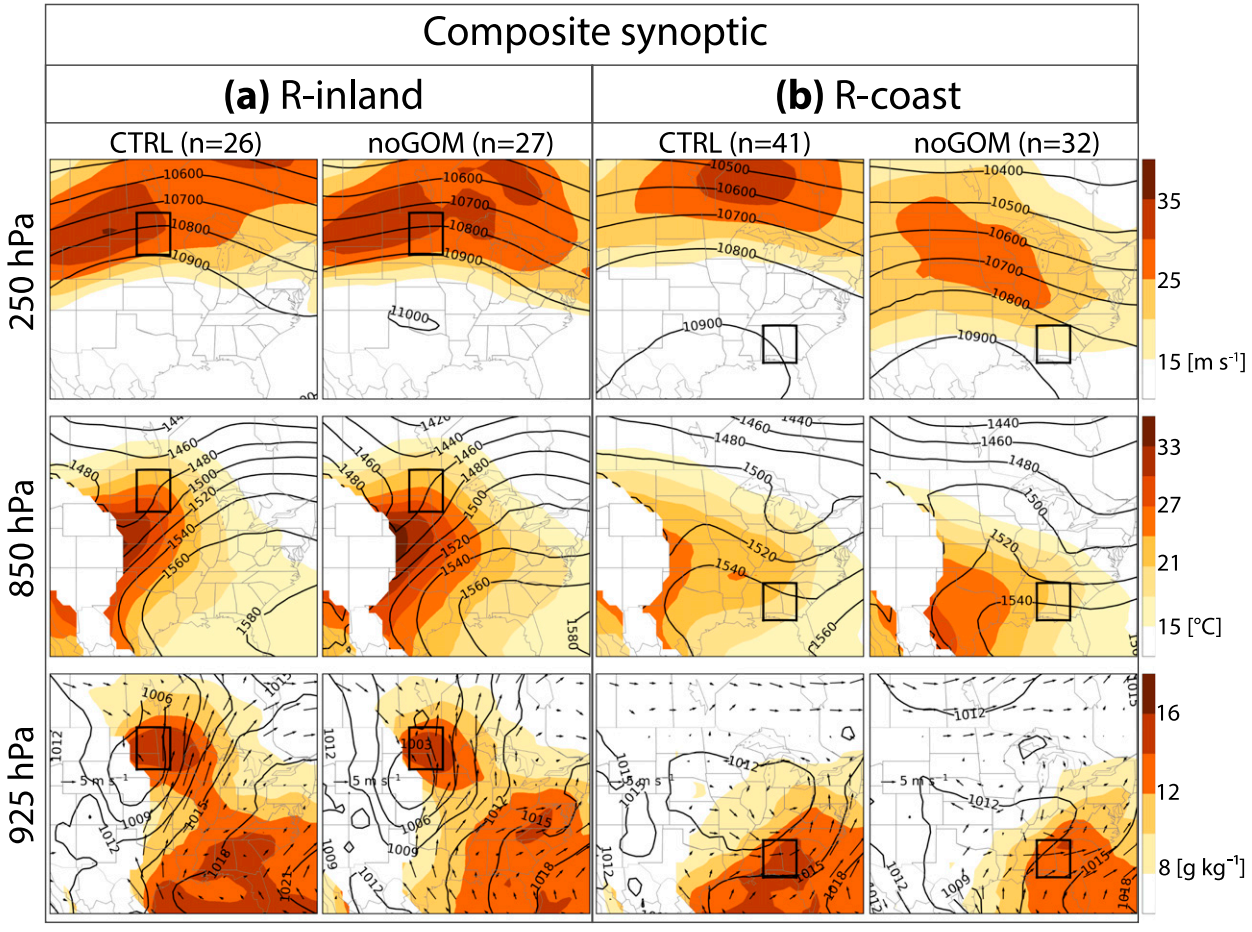

FIG. 14. CTRL vs noGOM for the composite synoptic patterns associated with extreme SLS environments in (a) R-inland and (b) R-coast. Plot aesthetics as in Fig. 8.

warming response in mean state is the strongest near the west Gulf coast and decreases in magnitude moving inland. Meanwhile, GPLLJs are increased over the deep south, which is consistent with the stronger low-level meridional winds, and thus partly contribute to the enhanced S06 and SRH03. The characteristic synoptic flow patterns that generate extreme SLS environments do not strongly depend on the Gulf of Mexico.

We also conducted an additional experiment with both North American topography removed and the Gulf of Mexico converted to land (Fig. S4). Responses in this experiment are broadly similar to responses in noTOPO, confirming that the presence of elevated terrain plays a critical role in producing downstream SLS environments as found over present-day North America, whereas the Gulf of Mexico plays a secondary role. The removal of these geographic components still leaves a residual peak of SLS environments near the southeast coast that decays inland and hence appears strongly driven by land–ocean contrast. The presence of the Gulf of Mexico shifts the primary local maximum of SLS environments westward closer to the elevated terrain, and acts as the essential moisture source for producing the secondary local maximum of these environments over the southern Great Plains. Thus, changes over the Gulf of Mexico (e.g., SST) may alter the spatial distribution of SLS environments; further investigation may provide insight into understanding changes in these environments observed in recent decades (Gensini and Brooks 2018; Tang et al. 2019; Taszarek et al. 2021a). Meanwhile, as noted earlier, although we filled the Gulf of Mexico with grassland in noGOM for simplicity, different land types may affect the details of these responses. Moreover, here we removed elevated terrain over all of North America in noTOPO, but specific topographic features, such as the Appalachian Mountains, may induce more localized responses; this could be a valuable avenue for future work. Note that extreme CAPES06 and EHI03 as defined here primarily represent high CAPE cases in spring and summer and hence are less representative of high shear, low CAPE environments that are more common in the cool seasons in the southeastern United States (Guyer and Dean 2010; Sherburn and Parker 2014; Sherburn et al. 2016; Li et al. 2020). Removing elevated terrain does lead to an increase in S06 during the winter, which may yield different responses to changes in elevated terrain on SLS environments in the cool

seasons. Finally, in addition to experiments with full-physics global climate models, idealized models with simplified settings could provide a more robust testing ground for understanding how surface properties control the formation of SLS environments on Earth.

Acknowledgments. We thank Editor Dr. Xin-Zhong Liang and three anonymous reviewers for their feedback in improving this manuscript. We would like to acknowledge high-performance computing support from Cheyenne (doi:10.5065/D6RX99HX) provided by NCAR's Computational and Information Systems Laboratory, sponsored by the National Science Foundation, for the simulations and data analysis performed in this work. We also acknowledge the open-source Python community, and particularly the authors and contributors to the Matplotlib (Hunter 2007), NumPy (Oliphant 2006), and MetPy (May et al. 2021) packages that were used to generate many of the analyses and figures. Li and Chavas were supported by NSF Grant AGS1648681. Reed was supported by NSF Grant AGS1648629. Rosenbloom was supported by the Regional and Global Model Analysis (RGMA) component of the Earth and Environmental System Modeling Program of the U.S. Department of Energy's Office of Biological and Environmental Research (BER) via National Science Foundation IA 1947282.

REFERENCES

Agard, V., and K. Emanuel, 2017: Clausius–Clapeyron scaling of peak CAPE in continental convective storm environments. *J. Atmos. Sci.*, **74**, 3043–3054, https://doi.org/10.1175/JAS-D-16-0352.1.

Agee, E., J. Larson, S. Childs, and A. Marmo, 2016: Spatial redistribution of U.S. tornado activity between 1954 and 2013. *J. Appl. Meteor. Climatol.*, **55**, 1681–1697, https://doi.org/10.1175/JAMC-D-15-0342.1.

Allen, J. T., and D. J. Karoly, 2014: A climatology of Australian severe thunderstorm environments 1979–2011: Inter-annual variability and ENSO influence. *Int. J. Climatol.*, **34**, 81–97, https://doi.org/10.1002/joc.3667.

Arritt, R. W., J. M. Wilczak, and G. S. Young, 1992: Observations and numerical modeling of an elevated mixed layer. *Mon. Wea. Rev.*, **120**, 2869–2880, https://doi.org/10.1175/1520-0493(1992)120<2869:OANMOA>2.0.CO;2.

Banacos, P. C., and M. L. Ekster, 2010: The association of the elevated mixed layer with significant severe weather events in the northeastern United States. *Wea. Forecasting*, **25**, 1082–1102, https://doi.org/10.1175/2010WAF2222363.1.

Barnes, S., and C. Newton, 1986: Thunderstorms in the synoptic setting. *Thunderstorm Morphology and Dynamics*, E. Kessler, Ed., University of Oklahoma Press, 75–111.

Benjamin, S. G., 1986: Some effects of surface heating and topography on the regional severe storm environment. Part II: Two-dimensional idealized experiments. *Mon. Wea. Rev.*, **114**, 330–343, https://doi.org/10.1175/1520-0493(1986)114<0330:SEOSHA>2.0.CO;2.

——, and T. N. Carlson, 1986: Some effects of surface heating and topography on the regional severe storm environment. Part I: Three-dimensional simulations. *Mon. Wea. Rev.*, **114**, 307–329, https://doi.org/10.1175/1520-0493(1986)114<0307:SEOSHA>2.0.CO;2.

Blackmon, M. L., 1976: A climatological spectral study of the 500 mb geopotential height of the Northern Hemisphere. *J. Atmos. Sci.*, **33**, 1607–1623, https://doi.org/10.1175/1520-0469(1976)033<1607:ACSSOT>2.0.CO;2.

Bogenschutz, P. A., A. Gettelman, H. Morrison, V. E. Larson, C. Craig, and D. P. Schanen, 2013: Higher-order turbulence closure and its impact on climate simulations in the Community Atmosphere Model. *J. Climate*, **26**, 9655–9676, https://doi.org/10.1175/JCLI-D-13-00075.1.

Bonner, W. D., 1968: Climatology of the low level jet. *Mon. Wea. Rev.*, **96**, 833–850, https://doi.org/10.1175/1520-0493(1968)096<0833:COTLLJ>2.0.CO;2.

Bony, S., J. L. Dufresne, H. Le Treut, J. J. Morcrette, and C. Senior, 2004: On dynamic and thermodynamic components of cloud changes. *Climate Dyn.*, **22**, 71–86, https://doi.org/10.1007/s00382-003-0369-6.

Brayshaw, D. J., B. Hoskins, and M. Blackburn, 2009: The basic ingredients of the North Atlantic storm track. Part I: Land–sea contrast and orography. *J. Atmos. Sci.*, **66**, 2539–2558, https://doi.org/10.1175/2009JAS3078.1.

Broccoli, A. J., and S. Manabe, 1992: The effects of orography on midlatitude Northern Hemisphere dry climates. *J. Climate*, **5**, 1181–1201, https://doi.org/10.1175/1520-0442(1992)005<1181:TEOOOM>2.0.CO;2.

Brooks, H. E., J. W. Lee, and J. P. Craven, 2003: The spatial distribution of severe thunderstorm and tornado environments from global reanalysis data. *Atmos. Res.*, **67–68**, 73–94, https://doi.org/10.1016/S0169-8095(03)00045-0.

Bunkers, M. J., B. A. Klimowski, J. W. Zeitler, R. L. Thompson, and M. L. Weisman, 2000: Predicting supercell motion using a new hodograph technique. *Wea. Forecasting*, **15**, 61–79, https://doi.org/10.1175/1520-0434(2000)015<0061:PSMUAN>2.0.CO;2.

Carlson, T. N., S. G. Benjamin, G. S. Forbes, and Y. F. Li, 1983: Elevated mixed layers in the regional severe storm environment: Conceptual model and case studies. *Mon. Wea. Rev.*, **111**, 1453–1474, https://doi.org/10.1175/1520-0493(1983)111<1453:EMLITR>2.0.CO;2.

Chang, E. K., 2009: Diabatic and orographic forcing of northern winter stationary waves and storm tracks. *J. Climate*, **22**, 670–688, https://doi.org/10.1175/2008JCLI2403.1.

Chavas, D. R., and D. T. Dawson II, 2020: An idealized physical model for the severe convective storm environmental sounding. *J. Atmos. Sci.*, **78**, 653–670, https://doi.org/10.1175/JAS-D-20-0120.1.

Chen, J., and D. R. Chavas, 2020: The transient responses of an axisymmetric tropical cyclone to instantaneous surface roughening and drying. *J. Atmos. Sci.*, **77**, 2807–2834, https://doi.org/10.1175/JAS-D-19-0320.1.

——, A. Dai, Y. Zhang, and K. L. Rasmussen, 2020: Changes in convective available potential energy and convective inhibition under global warming. *J. Climate*, **33**, 2025–2050, https://doi.org/10.1175/JCLI-D-19-0461.1.

Cheruy, F., J. Dufresne, F. Hourdin, and A. Ducharne, 2014: Role of clouds and land–atmosphere coupling in midlatitude continental summer warm biases and climate change amplification in CMIP5 simulations. *Geophys. Res. Lett.*, **41**, 6493–6500, https://doi.org/10.1002/2014GL061145.

Colby, F. P., Jr., 1984: Convective inhibition as a predictor of convection during AVE-SESAME II. *Mon. Wea. Rev.*, **112**, 2239–2252, https://doi.org/10.1175/1520-0493(1984)112<2239:CIAAPO>2.0.CO;2.

Cordeira, J. M., N. D. Metz, M. E. Howarth, and T. J. Galarneau Jr., 2017: Multiscale upstream and in situ precursors to the elevated mixed layer and high-impact weather over the Midwest United

States. *Wea. Forecasting*, **32**, 905–923, https://doi.org/10.1175/WAF-D-16-0122.1.

Davies-Jones, R. P., 1993: Helicity trends in tornado outbreaks. *17th Conf. on Severe Local Storms*, St. Louis, MO, Amer. Meteor. Soc., 56–60.

——, D. Burgess, and M. Foster, 1990: Test of helicity as a tornado forecast parameter. *16th Conf. on Severe Local Storms*, Kananaskis Park, AB, Canada, Amer. Meteor. Soc., 588–592.

Diffenbaugh, N. S., M. Scherer, and R. J. Trapp, 2013: Robust increases in severe thunderstorm environments in response to greenhouse forcing. *Proc. Natl. Acad. Sci. USA*, **110**, 16 361–16 366, https://doi.org/10.1073/pnas.1307758110.

Doswell, C. A., III, and E. N. Rasmussen, 1994: The effect of neglecting the virtual temperature correction on CAPE calculations. *Wea. Forecasting*, **9**, 625–629, https://doi.org/10.1175/1520-0434(1994)009<0625:TEONTV>2.0.CO;2.

——, and L. F. Bosart, 2001: Extratropical synoptic-scale processes and severe convection. *Severe Convective Storms*, C. A. Doswell, Ed., American Meteorological Society, 27–69.

——, and D. M. Schultz, 2006: On the use of indices and parameters in forecasting severe storms. *Electron. J. Severe Storms Meteor.*, **1** (3), https://www.ejssm.org/ojs/index.php/ejssm/article/viewArticle/11/12.

Doubler, D. L., J. A. Winkler, X. Bian, C. K. Walters, and S. Zhong, 2015: An NARR-derived climatology of southerly and northerly low-level jets over North America and coastal environs. *J. Appl. Meteor. Climatol.*, **54**, 1596–1619, https://doi.org/10.1175/JAMC-D-14-0311.1.

Duell, R. S., and M. S. Van Den Broeke, 2016: Climatology, synoptic conditions, and misanalyses of Mississippi River Valley drylines. *Mon. Wea. Rev.*, **144**, 927–943, https://doi.org/10.1175/MWR-D-15-0108.1.

Emori, S., and S. J. Brown, 2005: Dynamic and thermodynamic changes in mean and extreme precipitation under changed climate. *Geophys. Res. Lett.*, **32**, L17706, https://doi.org/10.1029/2005GL023272.

Eyring, V., S. Bony, G. A. Meehl, C. A. Senior, B. Stevens, R. J. Stouffer, and K. E. Taylor, 2016: Overview of the Coupled Model Intercomparison Project Phase 6 (CMIP6) experimental design and organization. *Geosci. Model Dev.*, **9**, 1937–1958, https://doi.org/10.5194/gmd-9-1937-2016.

Farrell, R. J., and T. N. Carlson, 1989: Evidence for the role of the lid and underrunning in an outbreak of tornadic thunderstorms. *Mon. Wea. Rev.*, **117**, 857–871, https://doi.org/10.1175/1520-0493(1989)117<0857:EFTROT>2.0.CO;2.

Fujita, T., 1958: Structure and movement of a dry front. *Bull. Amer. Meteor. Soc.*, **39**, 574–582, https://doi.org/10.1175/1520-0477-39.11.574.

Gates, W. L., and Coauthors, 1999: An overview of the results of the Atmospheric Model Intercomparison Project (AMIP I). *Bull. Amer. Meteor. Soc.*, **80**, 29–55, https://doi.org/10.1175/1520-0477(1999)080<0029:AOOTRO>2.0.CO;2.

Gensini, V. A., and W. S. Ashley, 2011: Climatology of potentially severe convective environments from the North American Regional Reanalysis. *Electron. J. Severe Storms Meteor.*, **6** (8), https://www.ejssm.org/ojs/index.php/ejssm/article/viewArticle/85.

——, and H. E. Brooks, 2018: Spatial trends in United States tornado frequency. *npj Climate Atmos. Sci.*, **1**, 38, https://doi.org/10.1038/s41612-018-0048-2.

——, T. L. Mote, and H. E. Brooks, 2014: Severe-thunderstorm reanalysis environments and collocated radiosonde observations. *J. Appl. Meteor. Climatol.*, **53**, 742–751, https://doi.org/10.1175/JAMC-D-13-0263.1.

Gettelman, A., and H. Morrison, 2015: Advanced two-moment bulk microphysics for global models. Part I: Off-line tests and comparison with other schemes. *J. Climate*, **28**, 1268–1287, https://doi.org/10.1175/JCLI-D-14-00102.1.

Golaz, J.-C., V. E. Larson, and W. R. Cotton, 2002: A PDF-based model for boundary layer clouds. Part I: Method and model description. *J. Atmos. Sci.*, **59**, 3540–3551, https://doi.org/10.1175/1520-0469(2002)059<3540:APBMFB>2.0.CO;2.

Grams, J. S., R. L. Thompson, D. V. Snively, J. A. Prentice, G. M. Hodges, and L. J. Reames, 2012: A climatology and comparison of parameters for significant tornado events in the United States. *Wea. Forecasting*, **27**, 106–123, https://doi.org/10.1175/WAF-D-11-00008.1.

Guyer, J. L., and A. R. Dean, 2010: Tornadoes within weak CAPE environments across the continental United States. *25th Conf. on Severe Local Storms*, Denver, CO, Amer. Meteor. Soc., 1.5, https://ams.confex.com/ams/pdfpapers/175725.pdf.

Hamill, T. M., R. S. Schneider, H. E. Brooks, G. S. Forbes, H. B. Bluestein, M. Steinberg, D. Meléndez, and R. M. Dole, 2005: The May 2003 extended tornado outbreak. *Bull. Amer. Meteor. Soc.*, **86**, 531–542, https://doi.org/10.1175/BAMS-86-4-531.

Hart, J. A., and W. Korotky, 1991: The SHARP workstation v1.50 users guide. National Weather Service, NOAA, U.S. Dept. of Commerce, 30 pp. [Available from NWS Eastern Region Headquarters, 630 Johnson Ave., Bohemia, NY 11716].

Harvey, B. J., L. C. Shaffrey, and T. J. Woollings, 2014: Equator-to-pole temperature differences and the extra-tropical storm track responses of the CMIP5 climate models. *Climate Dyn.*, **43**, 1171–1182, https://doi.org/10.1007/s00382-013-1883-9.

Held, I. M., M. Ting, and H. Wang, 2002: Northern winter stationary waves: Theory and modeling. *J. Climate*, **15**, 2125–2144, https://doi.org/10.1175/1520-0442(2002)015<2125:NWSWTA>2.0.CO;2.

Helfand, H. M., and S. D. Schubert, 1995: Climatology of the simulated Great Plains low-level jet and its contribution to the continental moisture budget of the United States. *J. Climate*, **8**, 784–806, https://doi.org/10.1175/1520-0442(1995)008<0784:COTSGP>2.0.CO;2.

Higgins, R. W., Y. Yao, E. S. Yarosh, J. E. Janowiak, and K. C. Mo, 1997: Influence of the Great Plains low-level jet on summertime precipitation and moisture transport over the central United States. *J. Climate*, **10**, 481–507, https://doi.org/10.1175/1520-0442(1997)010<0481:IOTGPL>2.0.CO;2.

Hoch, J., and P. Markowski, 2005: A climatology of springtime dryline position in the U.S. Great Plains region. *J. Climate*, **18**, 2132–2137, https://doi.org/10.1175/JCLI3392.1.

Holton, J. R., 1973: An introduction to dynamic meteorology. *Amer. J. Phys.*, **41**, 752–754, https://doi.org/10.1119/1.1987371.

Hoogewind, K. A., M. E. Baldwin, and R. J. Trapp, 2017: The impact of climate change on hazardous convective weather in the United States: Insight from high-resolution dynamical downscaling. *J. Climate*, **30**, 10 081–10 100, https://doi.org/10.1175/JCLI-D-16-0885.1.

Hunter, J. D., 2007: Matplotlib: A 2D graphics environment. *Comput. Sci. Eng.*, **9**, 90–95, https://doi.org/10.1109/MCSE.2007.55.

Inatsu, M., H. Mukougawa, and S.-P. Xie, 2002: Stationary eddy response to surface boundary forcing: Idealized GCM experiments. *J. Atmos. Sci.*, **59**, 1898–1915, https://doi.org/10.1175/1520-0469(2002)059<1898:SERTSB>2.0.CO;2.

Johns, R. H., 1993: Meteorological conditions associated with bow echo development in convective storms. *Wea. Forecasting*, **8**,

294–299, https://doi.org/10.1175/1520-0434(1993)008<0294:MCAWBE>2.0.CO;2.

——, and C. A. Doswell III, 1992: Severe local storms forecasting. *Wea. Forecasting*, **7**, 588–612, https://doi.org/10.1175/1520-0434(1992)007<0588:SLSF>2.0.CO;2.

Kaspi, Y., and T. Schneider, 2013: The role of stationary eddies in shaping midlatitude storm tracks. *J. Atmos. Sci.*, **70**, 2596–2613, https://doi.org/10.1175/JAS-D-12-082.1.

Klein, S. A., X. Jiang, J. Boyle, S. Malyshev, and S. Xie, 2006: Diagnosis of the summertime warm and dry bias over the U.S. Southern Great Plains in the GFDL climate model using a weather forecasting approach. *Geophys. Res. Lett.*, **33**, L18805, https://doi.org/10.1029/2006GL027567.

Lanicci, J. M., and T. T. Warner, 1991a: A synoptic climatology of the elevated mixed-layer inversion over the southern Great Plains in spring. Part I: Structure, dynamics, and seasonal evolution. *Wea. Forecasting*, **6**, 181–197, https://doi.org/10.1175/1520-0434(1991)006<0181:ASCOTE>2.0.CO;2.

——, and ——, 1991b: A synoptic climatology of the elevated mixed-layer inversion over the southern Great Plains in spring. Part II: The life cycle of the lid. *Wea. Forecasting*, **6**, 198–213, https://doi.org/10.1175/1520-0434(1991)006<0198:ASCOTE>2.0.CO;2.

——, and ——, 1991c: A synoptic climatology of the elevated mixed-layer inversion over the southern Great Plains in spring. Part III: Relationship to severe-storms climatology. *Wea. Forecasting*, **6**, 214–226, https://doi.org/10.1175/1520-0434(1991)006<0214:ASCOTE>2.0.CO;2.

Lawrence, D., and Coauthors, 2018: Technical description of version 5.0 of the Community Land Model (CLM). National Center for Atmospheric Research (NCAR), NCAR Tech. Note NCAR/TN-478+ STR, 257 pp., http://www.cesm.ucar.edu/models/cesm2/land/CLM50_Tech_Note.pdf.

Li, F., D. R. Chavas, K. A. Reed, and D. T. Dawson II, 2020: Climatology of severe local storm environments and synoptic-scale features over North America in ERA5 reanalysis and CAM6 simulation. *J. Climate*, **33**, 8339–8365, https://doi.org/10.1175/JCLI-D-19-0986.1.

Lin, Y., W. Dong, M. Zhang, Y. Xie, W. Xue, J. Huang, and Y. Luo, 2017: Causes of model dry and warm bias over central U.S. and impact on climate projections. *Nat. Commun.*, **8**, 881, https://doi.org/10.1038/s41467-017-01040-2.

Ludlam, F., 1963: Severe local storms: A review. *Severe Local Storms, Meteor. Monogr.*, No. 27, Amer. Meteor. Soc., 1–32, https://doi.org/10.1007/978-1-940033-56-3_1.

Lutsko, N. J., J. W. Baldwin, and T. W. Cronin, 2019: The impact of large-scale orography on Northern Hemisphere winter synoptic temperature variability. *J. Climate*, **32**, 5799–5814, https://doi.org/10.1175/JCLI-D-19-0129.1.

Markowski, P., and Y. Richardson, 2011: *Mesoscale Meteorology in Midlatitudes*. John Wiley & Sons, 430 pp.

May, R. M., S. C. Arms, P. Marsh, E. Bruning, J. R. Leeman, K. Goebbert, J. E. Thielen, and Z. S. Bruick, 2021: MetPy: A Python package for meteorological data. Unidata, https://doi.org/10.5065/D6WW7G29.

Mercer, A. E., M. B. Richman, C. A. Doswell III, C. M. Shafer, and L. M. Leslie, 2012: Synoptic composites of tornadic and non-tornadic outbreaks. *Mon. Wea. Rev.*, **140**, 2590–2608, https://doi.org/10.1175/MWR-D-12-00029.1.

Miller, P. W., and T. L. Mote, 2017: A climatology of weakly forced and pulse thunderstorms in the southeast United States. *J. Appl. Meteor. Climatol.*, **56**, 3017–3033, https://doi.org/10.1175/JAMC-D-17-0005.1.

Molina, M. J., and J. T. Allen, 2019: Regionally-stratified tornadoes: Moisture source physical reasoning and climate trends. *Wea. Climate Extremes*, **28**, 100244, https://doi.org/10.1016/j.wace.2020.100244.

——, and ——, 2020: On the moisture origins of tornadic thunderstorms. *J. Climate*, **32**, 4321–4346, https://doi.org/10.1175/JCLI-D-18-0784.1.

Mueller, B., and S. I. Seneviratne, 2014: Systematic land climate and evapotranspiration biases in CMIP5 simulations. *Geophys. Res. Lett.*, **41**, 128–134, https://doi.org/10.1002/2013GL058055.

Neale, R. B., J. H. Richter, and M. Jochum, 2008: The impact of convection on ENSO: From a delayed oscillator to a series of events. *J. Climate*, **21**, 5904–5924, https://doi.org/10.1175/2008JCLI2244.1.

——, and Coauthors, 2012: Description of the NCAR Community Atmosphere Model: CAM5.0. Tech. Rep. NCAR/TN-486+STR, National Center for Atmospheric Research, 268 pp., www.cesm.ucar.edu/models/cesm1.0/cam/docs/description/cam5_desc.pdf.

Oliphant, T. E., 2006: *A Guide to NumPy*. Trelgol Publishing, 261 pp.

Pan, Z., M. Segal, and R. W. Arritt, 2004: Role of topography in forcing low-level jets in the central United States during the 1993 flood-altered terrain simulations. *Mon. Wea. Rev.*, **132**, 396–403, https://doi.org/10.1175/1520-0493(2004)132<0396:ROTIFL>2.0.CO;2.

Parish, T. R., 2000: Forcing of the summertime low-level jet along the California coast. *J. Appl. Meteor.*, **39**, 2421–2433, https://doi.org/10.1175/1520-0450(2000)039<2421:FOTSLL>2.0.CO;2.

Qian, Y., and Coauthors, 2020: Neglecting irrigation contributes to the simulated summertime warm-and-dry bias in the central United States. *npj Climate Atmos. Sci.*, **3**, 1–10, https://doi.org/10.1038/s41612-020-00135-w.

Rasmussen, E. N., 2003: Refined supercell and tornado forecast parameters. *Wea. Forecasting*, **18**, 530–535, https://doi.org/10.1175/1520-0434(2003)18<530:RSATFP>2.0.CO;2.

——, and D. O. Blanchard, 1998: A baseline climatology of sounding-derived supercell and tornado forecast parameters. *Wea. Forecasting*, **13**, 1148–1164, https://doi.org/10.1175/1520-0434(1998)013<1148:ABCOSD>2.0.CO;2.

Rasmussen, K., and R. Houze Jr., 2016: Convective initiation near the Andes in subtropical South America. *Mon. Wea. Rev.*, **144**, 2351–2374, https://doi.org/10.1175/MWR-D-15-0058.1.

Reitan, C. H., 1974: Frequencies of cyclones and cyclogenesis for North America, 1951–1970. *Mon. Wea. Rev.*, **102**, 861–868, https://doi.org/10.1175/1520-0493(1974)102<0861:FOCACF>2.0.CO;2.

Ribeiro, B. Z., and L. F. Bosart, 2018: Elevated mixed layers and associated severe thunderstorm environments in South and North Americas. *Mon. Wea. Rev.*, **146**, 3–28, https://doi.org/10.1175/MWR-D-17-0121.1.

Richter, J. H., and P. J. Rasch, 2008: Effects of convective momentum transport on the atmospheric circulation in the Community Atmosphere Model, version 3. *J. Climate*, **21**, 1487–1499, https://doi.org/10.1175/2007JCLI1789.1.

Riemann-Campe, K., K. Fraedrich, and F. Lunkeit, 2009: Global climatology of convective available potential energy (CAPE) and convective inhibition (CIN) in ERA-40 reanalysis. *Atmos. Res.*, **93**, 534–545, https://doi.org/10.1016/j.atmosres.2008.09.037.

Rietkerk, M., and Coauthors, 2011: Local ecosystem feedbacks and critical transitions in the climate. *Ecol. Complex.*, **8**, 223–228, https://doi.org/10.1016/j.ecocom.2011.03.001.

Russell, D. R., 2006: Development of a time-domain, variable-period surface-wave magnitude measurement procedure for

application at regional and teleseismic distances, Part I: Theory. *Bull. Seismol. Soc. Amer.*, **96**, 665–677, https://doi.org/10.1785/0120050055.

Sandu, I., and Coauthors, 2019: Impacts of orography on large-scale atmospheric circulation. *npj Climate Atmos. Sci.*, **2**, 31, https://doi.org/10.1038/s41612-019-0065-9.

Schaefer, J. T., 1974: The life cycle of the dryline. *J. Appl. Meteor.*, **13**, 444–449, https://doi.org/10.1175/1520-0450(1974)013<0444:TLCOTD>2.0.CO;2.

Schemm, S., and T. Schneider, 2018: Eddy lifetime, number, and diffusivity and the suppression of eddy kinetic energy in midwinter. *J. Climate*, **31**, 5649–5665, https://doi.org/10.1175/JCLI-D-17-0644.1.

Seeley, J. T., and D. M. Romps, 2015: The effect of global warming on severe thunderstorms in the United States. *J. Climate*, **28**, 2443–2458, https://doi.org/10.1175/JCLI-D-14-00382.1.

Sherburn, K. D., and M. D. Parker, 2014: Climatology and ingredients of significant severe convection in high-shear, low-CAPE environments. *Wea. Forecasting*, **29**, 854–877, https://doi.org/10.1175/WAF-D-13-00041.1.

——, ——, J. R. King, and G. M. Lackmann, 2016: Composite environments of severe and nonsevere high-shear, low-CAPE convective events. *Wea. Forecasting*, **31**, 1899–1927, https://doi.org/10.1175/WAF-D-16-0086.1.

Staver, A. C., S. Archibald, and S. Levin, 2011: Tree cover in sub-Saharan Africa: Rainfall and fire constrain forest and savanna as alternative stable states. *Ecology*, **92**, 1063–1072, https://doi.org/10.1890/10-1684.1.

Tang, B. H., V. A. Gensini, and C. R. Homeyer, 2019: Trends in United States large hail environments and observations. *npj Climate Atmos. Sci.*, **2**, 45, https://doi.org/10.1038/s41612-019-0103-7.

Taszarek, M., H. E. Brooks, B. Czernecki, P. Szuster, and K. Fortuniak, 2018: Climatological aspects of convective parameters over Europe: A comparison of ERA-Interim and sounding data. *J. Climate*, **31**, 4281–4308, https://doi.org/10.1175/JCLI-D-17-0596.1.

——, J. T. Allen, T. Púčik, K. A. Hoogewind, and H. E. Brooks, 2020: Severe convective storms across Europe and the United States. Part II: ERA5 environments associated with lightning, large hail, severe wind, and tornadoes. *J. Climate*, **33**, 10 263–10 286, https://doi.org/10.1175/JCLI-D-20-0346.1.

——, ——, H. E. Brooks, N. Pilguj, and B. Czernecki, 2021a: Differing trends in United States and European severe thunderstorm environments in a warming climate. *Bull. Amer. Meteor. Soc.*, **102**, E296–E322, https://doi.org/10.1175/BAMS-D-20-0004.1.

——, N. Pilguj, J. T. Allen, V. Gensini, H. E. Brooks, and P. Szuster, 2021b: Comparison of convective parameters derived from ERA5 and MERRA2 with rawinsonde data over Europe and North America. *J. Climate*, **34**, 3211–3237, https://doi.org/10.1175/JCLI-D-20-0484.1.

Ting, M., and H. Wang, 2006: The role of the North American topography on the maintenance of the Great Plains summer low-level jet. *J. Atmos. Sci.*, **63**, 1056–1068, https://doi.org/10.1175/JAS3664.1.

Tippett, M. K., J. T. Allen, V. A. Gensini, and H. E. Brooks, 2015: Climate and hazardous convective weather. *Curr. Climate Change Rep.*, **1**, 60–73, https://doi.org/10.1007/s40641-015-0006-6.

——, C. Lepore, and J. E. Cohen, 2016: More tornadoes in the most extreme U.S. tornado outbreaks. *Science*, **354**, 1419–1423, https://doi.org/10.1126/science.aah7393.

Tochimoto, E., and H. Niino, 2015: Structural and environmental characteristics of extratropical cyclones that cause tornado outbreaks in the warm sector: A composite study. *Mon. Wea. Rev.*, **144**, 945–969, https://doi.org/10.1175/MWR-D-15-0015.1.

Trapp, R. J., N. S. Diffenbaugh, H. E. Brooks, M. E. Baldwin, E. D. Robinson, and J. S. Pal, 2007: Changes in severe thunderstorm environment frequency during the 21st century caused by anthropogenically enhanced global radiative forcing. *Proc. Natl. Acad. Sci. USA*, **104**, 19 719–19 723, https://doi.org/10.1073/pnas.0705494104.

Ulbrich, U., J. G. Pinto, H. Kupfer, G. C. Leckebusch, T. Spangehl, and M. Reyers, 2008: Changing Northern Hemisphere storm tracks in an ensemble of IPCC climate change simulations. *J. Climate*, **21**, 1669–1679, https://doi.org/10.1175/2007JCLI1992.1.

Ullrich, P. A., and C. M. Zarzycki, 2017: TempestExtremes: A framework for scale-insensitive pointwise feature tracking on unstructured grids. *Geosci. Model Dev.*, **10**, 1069–1090, https://doi.org/10.5194/gmd-10-1069-2017.

Varuolo-Clarke, A. M., K. A. Reed, and B. Medeiros, 2019: Characterizing the North American monsoon in the Community Atmosphere Model: Sensitivity to resolution and topography. *J. Climate*, **32**, 8355–8372, https://doi.org/10.1175/JCLI-D-18-0567.1.

Walters, C. K., J. A. Winkler, R. P. Shadbolt, J. van Ravensway, and G. D. Bierly, 2008: A long-term climatology of southerly and northerly low-level jets for the central United States. *Ann. Assoc. Amer. Geogr.*, **98**, 521–552, https://doi.org/10.1080/00045600802046387.

Weaver, S. J., and S. Nigam, 2008: Variability of the Great Plains low-level jet: Large-scale circulation context and hydroclimate impacts. *J. Climate*, **21**, 1532–1551, https://doi.org/10.1175/2007JCLI1586.1.

——, S. Baxter, and A. Kumar, 2012: Climatic role of North American low-level jets on U.S. regional tornado activity. *J. Climate*, **25**, 6666–6683, https://doi.org/10.1175/JCLI-D-11-00568.1.

Wehner, M. F., and Coauthors, 2014: The effect of horizontal resolution on simulation quality in the Community Atmospheric Model, CAM5.1. *J. Adv. Model. Earth Syst.*, **6**, 980–997, https://doi.org/10.1002/2013MS000276.

Weisman, M. L., and R. Rotunno, 2000: The use of vertical wind shear versus helicity in interpreting supercell dynamics. *J. Atmos. Sci.*, **57**, 1452–1472, https://doi.org/10.1175/1520-0469(2000)057<1452:TUOVWS>2.0.CO;2.

Whiteman, C. D., X. Bian, and S. Zhong, 1997: Low-level jet climatology from enhanced rawinsonde observations at a site in the southern Great Plains. *J. Appl. Meteor.*, **36**, 1363–1376, https://doi.org/10.1175/1520-0450(1997)036<1363:LLJCFE>2.0.CO;2.

Williams, E., and N. Renno, 1993: An analysis of the conditional instability of the tropical atmosphere. *Mon. Wea. Rev.*, **121**, 21–36, https://doi.org/10.1175/1520-0493(1993)121<0021:AAOTCI>2.0.CO;2.

Wilson, C., B. Sinha, and R. G. Williams, 2009: The effect of ocean dynamics and orography on atmospheric storm tracks. *J. Climate*, **22**, 3689–3702, https://doi.org/10.1175/2009JCLI2651.1.

Zarzycki, C., 2018: Projecting changes in societally impactful northeastern US snowstorms. *Geophys. Res. Lett.*, **45**, 12 067–12 075, https://doi.org/10.1029/2018GL079820.

Zhang, G. J., and N. A. McFarlane, 1995: Sensitivity of climate simulations to the parameterization of cumulus convection in the Canadian Climate Centre general circulation model. *Atmos.–Ocean*, **33**, 407–446, https://doi.org/10.1080/07055900.1995.9649539.

Ziegler, C. L., and C. E. Hane, 1993: An observational study of the dryline. *Mon. Wea. Rev.*, **121**, 1134–1151, https://doi.org/10.1175/1520-0493(1993)121<1134:AOSOTD>2.0.CO;2.

Zishka, K. M., and P. J. Smith, 1980: The climatology of cyclones and anticyclones over North America and surrounding ocean environs for January and July, 1950–77. *Mon. Wea. Rev.*, **108**, 387–401, https://doi.org/10.1175/1520-0493(1980)108<0387:TCOCAA>2.0.CO;2.